AMERICAN SOCIETY FOR MICROBIOLOGY | Journal of Virology

Hepatitis C Virus Is Released via a Noncanonical Secretory Route

Karen Bayer,[a] Carina Banning,[c] Volker Bruss,[a] Linda Wiltzer-Bach,[b] Michael Schindler[a,b,c]

Institute of Virology, Helmholtz Zentrum München-German Research Center for Environmental Health, Munich, Germany[a]; University Hospital Tübingen, Institute for Medical Virology and Epidemiology of Viral Diseases, Tübingen, Germany[b]; Heinrich Pette Institute, Leibniz Institute for Experimental Virology, Hamburg, Germany[c]

ABSTRACT

We analyzed hepatitis C virus (HCV) morphogenesis using viral genomes encoding a mCherry-tagged E1 glycoprotein. HCV-E1-mCherry polyprotein expression, intracellular localization, and replication kinetics were comparable to those of untagged HCV, and E1-mCherry-tagged viral particles were assembled and released into cell culture supernatants. Expression and localization of structural E1 and nonstructural NS5A followed a temporospatial pattern with a succinct decrease in the number of replication complexes and the appearance of E1-mCherry punctae. Interaction of the structural proteins E1, Core, and E2 increased at E1-mCherry punctae in a time-dependent manner, indicating that E1-mCherry punctae represent assembled or assembling virions. E1-mCherry did not colocalize with Golgi markers. Furthermore, the bulk of viral glycoproteins within released particles revealed an EndoH-sensitive glycosylation pattern, indicating an absence of viral glycoprotein processing by the Golgi apparatus. In contrast, HCV-E1-mCherry trafficked with Rab9-positive compartments and inhibition of endosomes specifically suppressed HCV release. Our data suggest that assembled HCV particles are released via a noncanonical secretory route involving the endosomal compartment.

IMPORTANCE

The goal of this study was to shed light on the poorly understood trafficking and release routes of hepatitis C virus (HCV). For this, we generated novel HCV genomes which resulted in the production of fluorescently labeled viral particles. We used live-cell microscopy and other imaging techniques to follow up on the temporal dynamics of virus particle formation and trafficking in HCV-expressing liver cells. While viral particles and viral structural protein were found in endosomal compartments, no overlap of Golgi structures could be observed. Furthermore, biochemical and inhibitor-based experiments support a HCV release route which is distinguishable from canonical Golgi-mediated secretion. Since viruses hijack cellular pathways to generate viral progeny, our results point toward the possible existence of a not-yet-described cellular secretion route.

Hepatitis C virus (HCV) belongs to the *Flavivirus* genus and has a positive-strand RNA genome. This encodes a polyprotein which is posttranslationally cleaved into six nonstructural (NS) proteins, the ion channel p7 protein, and the structural proteins Core, E1, and E2 (1). The NS proteins reside at the outer leaflet of the endoplasmic reticulum (ER) membrane where NS4B and NS5A in particular induce membrane alterations resulting in the formation of the membranous web, which is the major site for HCV replication (2–5). Core is targeted to adjacent lipid droplets (LDs) (6, 7), which represent intracellular lipid deposits and are considered important for production of infectious particles (1, 7, 8). The E1 and E2 envelope proteins are incorporated into ER membranes with ectodomains facing the ER lumen (9, 10). Later, they are recruited to assembly sites via the NS2 complex (11, 12). Upon recruitment of all required viral components, HCV assembly is thought to occur at the surface of LDs (6–8, 13).

The mechanisms that trigger switching from polyprotein translation to viral RNA (vRNA) replication and then to the initiation of virus assembly are largely unknown. Recently, it has been proposed that the cellular Ewing sarcoma breakpoint region 1 (EWSR1) protein is important for regulation of the switch from translation to replication by binding to the *cis*-acting replication element of HCV (14). Furthermore, transport of HCV Core toward LDs by the enzyme diacylglycerol acyltransferase-1 (DGAT1) is crucial for production of newly formed virions (15, 16), and the NS2 protein, together with p7, might be a major player in coordinating assembly (11, 17, 18).

How HCV is released from infected cells is still under debate. HCV was found to associate with constituents of very-low-density lipoproteins (VLDL), such as ApoB and ApoE (19–21), and proteins of the VLDL secretory pathway, including the transcription factor hepatocyte nuclear factor 4 (HNF4) (22). Thus, it has been assumed that HCV budding, maturation, and release might intersect the VLDL secretion pathway (13), but a precise model is still lacking and a recent study suggested that HCV release is independent of the VLDL route (23).

Other members of the *Flaviviridae*, e.g., dengue virus and bovine viral diarrhea virus, are released through classical secretion via the Golgi apparatus and the *trans*-Golgi network (24–26). Therefore, a similar mechanism has been postulated for HCV. In a recent study, PI4P-binding protein GOLPH3 was suggested to have a role in HCV budding since silencing of this protein led to reduced levels of HCV release (27). Similarly, a small interfering

Received 16 August 2016 **Accepted** 11 September 2016

Accepted manuscript posted online 14 September 2016

Citation Bayer K, Banning C, Bruss V, Wiltzer-Bach L, Schindler M. 2016. Hepatitis C virus is released via a noncanonical secretory route. J Virol 90:10558–10573. doi:10.1128/JVI.01615-16.

Editor: J.-H. J. Ou, University of Southern California

Address correspondence to Michael Schindler, michael.schindler@med.uni-tuebingen.de.

Supplemental material for this article may be found at http://dx.doi.org/10.1128/JVI.01615-16.

RNA (siRNA) screen that targeted 140 cellular membrane trafficking genes has identified components of the classical secretion pathway that affected the release of HCV (28). However, silencing such cellular membrane trafficking genes might have effects on the processing of proteins that are involved in other, possibly as-yet-unknown intracellular trafficking and secretion pathways which could be essential to the release of HCV (29). Furthermore, such interventions are very likely to influence various cellular processes and signaling pathways. As an example, GOLPH3 is also a key player in modulation of mTOR signaling (30).

In order to investigate the process of HCV assembly, budding, and release, we constructed HCV genomes with a fluorescent tag within the E1 protein [Jc1-E1(A4)-mCherry]. We also inserted this tag in combination with a previously described green fluorescent protein (GFP)-tagged NS5A genome (31), generating the Jc1-E1(A4)-mCherry/NS5A-GFP virus, which allows simultaneous visualization of structural protein expression and replication complexes (RCs). Live-cell observations and confocal microscopy of HCV-expressing Huh7.5 cells revealed a distinct temporospatial organization of structural (E1) and nonstructural (NS5A) protein expression. Detailed biochemical and microscopic analyses revealed the importance of the endosomal compartment for HCV egress and an unconventional secretory route hijacked by HCV for release.

MATERIALS AND METHODS

HCV constructs and expression plasmids. The following HCV constructs were kind gifts from R. Bartenschlager (University of Heidelberg): pFK_Jc1 (32), pFK_Jc1-luc (32), pFK_Jc1-Flag-E2 (33), and pFK_Jc1-NS5A-GFP (31). To generate HCV with a fluorescently labeled structural protein (pFK_Jc1-E1-mCherry), we amplified mCherry (primers 5′mCherry-*BsiWI* [5′-GGCGTACGCGATGGTGAGCAAGGGCGAG-3′] and 3′mCherry-*BsiWI* [5′-CGCGTACGCCTTGTACAGCTCGTCCATGCC-3′]) and introduced flanking BsiWI restriction sites and then ligated mCherry into the BsiWI site present between the last glycosylation site and the transmembrane domain of E1 in pFK_Jc1. The nucleotide sequence was confirmed by Sanger sequencing. The double-labeled HCV genome expressing E1-mCherry and NS5A-GFP (pFK_Jc1-E1-mCherry/NS5A-GFP) was generated by the same cloning strategy, but mCherry was inserted into pFK_Jc1-NS5A-GFP. The variants with the reconstituted HCV H77 E1-A4 epitope sequence (34) were generated by initial reconstitution of the A4 epitope in the pFK_Jc1 by site-directed mutagenesis. The other variants were then cloned as described above. A yellow fluorescent protein (YFP) fusion construct of the secreted Gaussia luciferase (35) was constructed by PCR amplification (primers 5′Gaussia NheI [5′-CCGGCTAGCATGGGAGTCAAAGTTCTGTTTG-3′] and 3′Gaussia AgeI [5′-TCGACCGGTGCACCTGCTCCGTCACCACCGGCCCCCTTGATC-3′]) and ligation into the Clontech vector pEYFP-N1 as described before (36). Similarly, we constructed the pECFP-CD74 expression vector. The mCherry-hepatitis B virus (HBV)-S construct was generated by fusing a sequence encoding the secretion signal of beta-lactamase to the 5′ end of the mCherry open reading frame and by further fusion of this chimera to the 5′end of the HBV-S gene using standard PCR techniques. A linker sequence coding for the peptide SLDPATSVDGGGGVDGGGGVEN was inserted between the mCherry- and HBV-S-derived portions. The cyan fluorescent protein (CFP)-GalT construct (37) was provided by P. Bastiaens (MPI, Dortmund, Germany). pOPIN(n)eCFP-Rab7A and pOPIN(n)eCFP-Rab9A were gifts from A. Musacchio (MPI, Dortmund, Germany), GFP-vesicular stomatitis virus G protein (GFP-VSVG) was a gift from F. Perez (Institut Curie, Paris, France), and GFP-ApoE was a gift from G. Randall (University of Chicago, Chicago, IL).

Cell culture, transfection, and HCV RNA electroporation. Huh7.5 cells (kindly provided by C. Rice, Rockefeller University) were cultured as previously described (38), and plasmids were coelectroporated with RNA of HCV Jc1 genomes using a Bio-Rad Gene Pulser Xcell system. *In vitro* transcription of HCV RNA and electroporation were performed as previously described (39, 40). Briefly, the pFK plasmids were linearized by MluI digestion, purified with a Wizard DNA Clean-Up system (Promega), and used for *in vitro* transcription with the help of a TranscriptAid T7 high-yield transcription kit (Fermentas). Both kits were used according to the manufacturer's instructions. The RNA was purified by phenol chloroform extraction and stored at −80°C. For electroporation, 6×10^6 cells and 5 μg RNA were used as previously described (40). Cells were then seeded in well plates, and the medium was changed after 6 h.

Infectivity assay. Huh7.5 cells (39×10^6) were electroporated with RNA of each construct and seeded into two 175-cm^2 flasks. Supernatants of both flasks were pooled at 65 h postelectroporation (hpe), and cell debris was removed by centrifugation at 3,000 rpm for 10 min before ultracentrifugation was performed using a 20% sucrose cushion at 28,000 rpm for 90 min at 4°C. Pellets were resuspended in 400 μl medium at 4°C overnight. Naive Huh7.5 cells were seeded in a 12-well plate (160,000 cells/well) and infected in a 400-μl volume for an incubation period of 6 h before cells were kept in fresh medium for 3 days. The cells were then trypsinized, washed in phosphate-buffered saline (PBS), and fixed in 2% paraformaldehyde (PFA) for 1 h at room temperature. Mock-infected cells were divided into two parts, one of which was stained for intracellular Core together with cells infected with Jc1-E1(A4). For this, cells were treated with 1% saponin for 12 min at room temperature, washed twice in PBS, and blocked in 10% goat serum for 20 min at room temperature before they were incubated with primary antibody (mouse anti-Core, clone C7-50; Abcam) at a 1:100 dilution for 1 h at room temperature. The secondary antibody (goat anti-mouse Alexa 633) was diluted 1:200 in 1% goat serum–PBS, cells were incubated for 1 h at room temperature and washed twice in PBS, and mean fluorescence intensity (MFI) was analyzed using a BD FACSCanto II or Aria-III system.

Virus purification and concentration. The supernatant of vRNA-electroporated cells was collected 72 hpe, and cell debris was pelleted by centrifugation for 10 min at 3,000 rpm. A 32-ml volume of cleared supernatant was transferred to an ultracentrifugation tube for the SW 28 rotor (Beckman Coulter). Each supernatant was carefully underlaid with 5 ml 20% sucrose–PBS and centrifuged using an Optima L7-65 Ultracentrifuge (Beckman Coulter) for 90 min at 28,000 rpm and 4°C. Pelleted virus was dissolved in PBS or medium (50 to 100 μl) and resuspended for 16 h at 4°C.

Fractionation of virus preparations. Gradient fractions were prepared by mixing decreasing amounts of serum-free medium with increasing amounts of iodixanol density medium (OptiPrep) to obtain fractions from 14%, 18%, 22%, 26%, 30%, 34%, and 38% iodixanol. Fractions were transferred to an ultracentrifugation tube and subsequently overlaid with the concentrated virus and centrifuged at 34,000 rpm and 4°C for 20 h in an Optima L7-65 Ultracentrifuge (Beckman Coulter). The recovered fractions were diluted 1:2 with PBS and centrifuged again at 21,000 × *g* at 4°C for 90 min to concentrate virus particles or proteins in a pellet for downstream applications.

Endoglycosidase digestion. Huh7.5 cells (18×10^6) were electroporated, cultured for 56 h in a 175-cm^2 flask, detached, washed, and lysed with 0.5% NP-40. In parallel, virus supernatant collected from 10 175-cm^2 flasks was concentrated via ultracentrifugation or additional gradient centrifugation and resuspended in 100 μl PBS (each). Glycoprotein denaturation buffer (NEB) (10 ×) was added to the supernatant after cell lysis or to virus-containing culture supernatant, and the reaction mixture was boiled at 95°C for 10 min. Samples were subdivided into three equal parts consisting of the untreated control samples and samples digested with EndoH (NEB) or with peptide:*N*-glycosidase F (PNGaseF) (NEB). Deglycosylation was done with the protocol provided by the manufacturer. Finally, 5× SDS loading buffer was added to the samples and, after boiling at 95°C was performed, they were further separated by SDS-PAGE and analyzed by Western blotting (WB).

Western blotting. At 2 to 3 days postelectroporation, HCV-producing Huh7.5 cells were pelleted, lysates were generated with standard radioimmunoprecipitation assay (RIPA) buffer, and proteins were separated by 12% SDS-PAGE. Expression of E2 and Core in whole-cell lysates was analyzed by WB using 1:500-diluted mouse anti-Core (clone C7-50; Abcam) or 1:100-diluted mouse anti-E2 AP33 antibody (provided by Genentech) (41). The anti-E1(A4) antibody was a kind gift from Harry Greenberg and used at a 1:1,000 dilution (34). The mouse anti-β-actin (clone AC-15; Sigma-Aldrich) (diluted 1:5,000) served as a loading control. mCherry was detected with a polyclonal rabbit antibody (BioVision) at a 1:1,000 dilution and the HBV-S protein with the mouse monoclonal HB1 antibody (kind gift from D. Glebe, Göttingen, Germany) at a 1:1,000 dilution. For secondary antibody staining, IRDye 800 goat anti-mouse and IRDye 680 goat anti-rabbit (Li-Cor Biotechnology GmbH) (diluted 1:5,000) or goat anti-mouse horseradish peroxidase (HRP) and goat anti-rabbit HRP (Dianova) (diluted 1:10,000) antibodies were used. Detection was performed using either chemiluminescence or an Odyssey infrared imaging system (Li-Cor).

Coimmunoprecipitation. Huh7.5 cells (18×10^6) were electroporated with viral RNA, detached 56 hpe, and washed with cold PBS. Cells were sheared through a syringe in 800 μl CoIP lysis buffer (0.05 M Tris, 0.15 M NaCl, 1 mM EDTA [pH 7.4], 1% Triton X-100, and fresh protease inhibitor) and rotated on a wheel for 20 min at 4°C before centrifugation of cell debris was performed at 17,000 × *g* for 10 min. The agarose matrix coupled with anti-Flag tag antibodies (mouse anti-Flag; Sigma-Aldrich) was washed twice with CoIP wash buffer (0.05 M Tris, 0.15 M NaCl, pH 7.4) and once with 0.1 M glycine (pH 3.5) to remove unbound antibodies. After washing with CoIP wash buffer was performed, the cleared protein-containing supernatant and protease inhibitor (Roche) were added to 30 μl of the matrix and incubated on a wheel overnight at 4°C. Thereafter, the matrix was washed for removal of unspecific bound protein. Proteins were released from the matrix by the use of 20 μl 5× SDS loading buffer (250 mM Tris-HCl [pH 6.8], 50% glycerol, 15% SDS, 0.01% bromophenol blue, 25% β-mercaptoethanol) and 5 min of boiling at 95°C. Proteins in the precipitates were separated by SDS-PAGE and detected by WB.

Flow cytometry and intracellular Core detection. Cells were detached with trypsin-EDTA, washed twice with PBS in fluorescence-activated cell sorter (FACS) tubes, fixed for 20 min in 2% PFA, and permeabilized for 10 min at room temperature in 1% saponin–PBS. The reaction mixture was then washed twice and blocked with 10% goat serum–PBS for 30 min at room temperature. Cells were stained with primary antibody dilution (mouse anti-Core; Abcam) diluted 1:100 in 1% goat serum–PBS for 1 h at 4°C. After three washing steps, cells were incubated with secondary antibody (Alexa Fluor 633 goat anti-mouse; Life Technologies) diluted 1:500 in 1% goat serum–PBS at 4°C in the dark. After washing was performed, cells were analyzed using a BD FACSCanto II or Aria-III system.

Quantitative RT-PCR. For quantitative reverse transcription-PCR (qRT-PCR) measurement of vRNA isolated by the use of a NucleoSpin RNA kit (Macherey-Nagel), we used a OneStep RT-PCR kit (Qiagen), which reverse transcribes and amplifies the RNA in the same reaction mixture, according to the manufacturer's instructions. We used the sample RNA and predefined standard dilution series of *in vitro*-transcribed HCV RNA and HCV-5′ noncoding region-specific primers (HCV fw [5′-GCTAGCCGAGTAGCGTTGGGT-3′] and HCV rev [5′-TGCTCATGG TGCACGGTCTACC-3′]) as well as the DNA probe (5′-6-carboxyfluorescein [FAM]-TACTGCCTGATAGGGCGCTTGCGAGTG-6-carboxytetramethylrhodamine [TAMRA]-3′) for RT-PCR measurements performed with a LightCycler 480 instrument (Roche). The absolute quantification was performed with the help of a standard curve and the calculation of the absolute number of viral RNA copies within the samples.

Virus release and Gaussia secretion assay. To study virus release, we used the Jc1-luc reporter virus (32). As a control, a similar experiment was performed with cells expressing Gaussia luciferase. Huh7.5 cells were electroporated with vRNA or a plasmid coding for a YFP-fused Gaussia luciferase construct. Cells were cultured for 2 days, and medium was removed, cells were washed with PBS, and inhibitor-containing medium was added. All inhibitors were dissolved in dimethyl sulfoxide (DMSO) and used at the following concentrations, which were found to be nontoxic for Huh7.5 cells by MTT [3-(4,5-dimethyl-2-thiazolyl)-2,5-diphenyl-2H-tetrazolium bromide] testing: brefeldin A (AppliChem) at 5 μg/ml and U18666A (Cayman Chemical) at 25 μM. At 8 h postincubation, virus-containing supernatants were harvested and viral particles were purified to remove the inhibitors. A 20% sucrose cushion was carefully overlaid with supernatant and centrifuged for 90 min at 20,000 × *g* and 4°C. The supernatant was withdrawn with a pipette without touching the pellet, and the virus pellet was resuspended in fresh medium. These cleared virus supernatants were used to inoculate Huh7.5 cells in a 96-well format. At 3 days later, luciferase activity was assessed with a luciferase assay system (Promega) according to the manufacturer's instructions. Gaussia luciferase activity in the supernatant was measured directly with a BioLux Gaussia Luciferase Flex assay kit (NEB) as recommended by the manufacturer.

Biochemical fixation of the early endosomal compartment. The biochemical fixation of horseradish peroxidase (HRP)-containing compartments has been described before (42, 43). We used that system to inactivate the early endosomal compartment as follows: at 2 days postelectroporation, HCV Jc1-luc- or Gaussia luciferase-expressing cells were starved for 90 min with medium containing 0.1% fetal calf serum (FCS). The cells were then incubated for 2 h at room temperature with medium containing 0.1% FCS, 20 mM HEPES, and 20 μg/ml transferrin (Tf) as a control or HRP-coupled transferrin (HRP-Tf), respectively. Cells were washed three times with cold PBS and incubated with 10% FCS-containing medium for 10 min. Subsequently, cells were kept on ice and diaminobenzidine (DAB) solution with 0.003% H_2O_2 was added for 60 min to inactivate the HRP-Tf-containing endosomes. After washing with cold PBS was performed, complete medium was added and cells were allowed to produce virus or secrete Gaussia luciferase for a further 5 h. The amount of released virus or secreted Gaussia luciferase was assessed as described above.

Immunofluorescence and proximity ligation assay. HCV vRNA-electroporated cells were grown in a 24-well plate on 12-mm-diameter coverslips and stained after the indicated time points. In brief, cells were washed and fixed for 20 min at 4°C with 2% PFA. Some samples were directly mounted using Mowiol 4-88 (Roth) or permeabilized for 10 min at room temperature with 1% saponin and blocked with 10% goat serum–PBS for 30 min at room temperature. Primary antibodies were diluted 1:100 in 1% goat serum–PBS and incubated within a humid environment for 2 h at room temperature. Samples were washed to remove unbound antibodies and incubated with secondary antibodies (Alexa Fluor 488, Alexa Fluor 555, or Alexa Fluor 633 goat anti-mouse; Life Technologies) diluted 1:200 in 1% goat serum–PBS for 1 h at room temperature in the dark. After washing was performed, coverslips were mounted with Mowiol 4-88 (Roth), dried at room temperature for 16 h in the dark, and analyzed by spinning-disc confocal fluorescence microscopy (Nikon Ti Eclipse microscope with an UltraView VoX system; PerkinElmer). For proximity ligation assay (PLA), cells were permeabilized and fixed as described above, but blocking was done for 45 min with 5% bovine serum albumin (BSA). Immunodetection was done with primary antibodies from rabbit directed against mCherry (BioVision) and mouse anti-E2 (AP-33), anti-Core (C7-50; Abcam), anti-NS3 (clone F3A6B2C3 against epitopes 1322 to 1662 of JFH-1 NS3), or anti-NS5A (2F6/G11; IBT) diluted 1:100 in 1% BSA–PBS for 2 h at room temperature. Afterwards, samples were prepared according to the protocol of the manufacturer (Duolink; Sigma-Aldrich) and as described previously (18). Spots of the fluorescent substrate were detected by confocal spinning-disc microscopy (Nikon Ti Eclipse microscope with an UltraView VoX system; PerkinElmer). Quantitative analyses were performed using the Volocity software-implemented automated spot-counting tool with a defined maximum spot size of 0.8 μm.

Live-cell imaging and fluorescence recovery after photobleaching (FRAP). Microscopy was performed with a fully motorized Nikon Ti Eclipse inverted microscope equipped with a hardware-based perfect-focus system and a PerkinElmer UltraView VoX spinning-disc system. If not indicated otherwise, 0.45×10^6 Huh7.5 cells electroporated with RNA of the HCV Jc1 genomes were seeded in a 35-mm-diameter dish with an optical bottom (Ibidi or WillCo) and cultivated for the indicated times. Microscopy was performed in a humidified chamber with 5% CO_2 at 37°C, and a CFI Apochromat 60× objective (numerical aperture [NA], 1.49) was used for imaging. Video sequences were processed using Volocity software. FRAP areas were selected by placing regions of interest and respective areas with background fluorescence. Time lapse imaging was started before bleaching in 3- to 5-s intervals and continued for approximately 5 min, depending on the experiment. Photobleaching was performed by a single pulse for 60 ms. Intensity profiles of the different areas were computed by the use of Volocity software and Excel software (Microsoft).

Image analysis and software. Microscopic sequences, colocalization analyses, and spot counting was performed using the Volocity version 6.2 software package (PerkinElmer). In general, images were never modified apart from enhancement of contrast and/or brightness. Movies were generated and data were compressed using the freely available ImageJ (Fiji) and VirtualDub V1.10.4 software packages. Statistical analyses were performed using the GraphPad Prism 5.0 and 6.0 software packages and the two-tailed Student's *t* test or multiple analyses of variance (ANOVA).

RESULTS

Construction and characterization of HCV genomes expressing fluorescently labeled E1 structural protein. To study HCV morphogenesis, the temporospatial dynamics of HCV structural protein expression, and the formation of replication complexes in living cells, we generated several HCV genomes expressing fluorescently labeled E1 protein (Fig. 1A). The mCherry red monomeric fluorescent protein (44) was inserted between the C-terminal glycosylation site of E1 and the stalk region of the transmembrane domain (see Materials and Methods for details). We also reconstituted the E1(A4) epitope from strain HCV H77, enabling detection of E1 by a monoclonal antibody (34). Using this strategy, we generated HCV Jc1 (32) expressing an E1-mCherry fusion protein [Jc1-E1(A4)-mCherry] as well as a variant coexpressing GFP within the NS5A protein [Jc1-E1(A4)-mCherry/NS5A-GFP] (Fig. 1A). Western blot analysis showed efficient expression of the viral proteins Core, E1(A4)-mCherry, and E2 (Fig. 1B). Furthermore, the subcellular localization of Core, NS5A, E2, and E1-mCherry in Huh7.5 cells electroporated with RNA of Jc1-E1(A4)-mCherry was comparable to viral protein localization in cells electroporated with RNA of Jc1-E1(A4) (Fig. 1C).

Since insertion of mCherry into E1 might affect growth kinetics, we characterized the novel HCV genomes in regard to viral replication and release of viral particles. First, we electroporated Huh7.5 cells with RNA of the indicated HCV Jc1-E1(A4) variants and fixed and stained for Core protein to assess the relative amounts of HCV-positive cells at different time points over 64 h hpe using flow cytometry. All Jc1-E1(A4) variants showed similar kinetics, with the amount of Core-positive cells increasing until 40 hpe (Fig. 2A). At later time points, the level of Core-positive cells of untagged Jc1-E1(A4) reached a plateau whereas kinetics for all the variants expressing chromophore-tagged viral proteins slowly decreased. Our explanation of this is that it occurred as a consequence of the strongly attenuated infectivity of the fluorescently labeled variants (Fig. 2B), while the untagged Jc1 is capable of multiple rounds of reinfection and therefore of spreading within the cell culture.

Within the population of Core-expressing cells, the levels of mean fluorescence intensity (MFI) of Core protein staining were comparable for all variants, indicating that the amounts of viral protein produced were similar (Fig. 2C). Also, the MFI of Core protein staining for all variants increased over time, suggesting that protein production within HCV-expressing cells was not impaired. To corroborate these results and to assess time-dependent expression of other viral structural proteins, we prepared cell lysates at the same time points for WB analysis. Similarly to the flow cytometry measurements, there was a clear increase in viral protein levels from 16 hpe to 48 hpe for Jc1-E1(A4) and Jc1-E1(A4)-mCherry/NS5A-GFP, not only for Core but also for the E1 and E2 viral glycoproteins (Fig. 2D).

To analyze production of vRNA over time, we extracted total RNA from cells and supernatants at 24, 40, 48, and 64 hpe and performed qRT-PCR. To calculate the level of vRNA production per HCV-expressing cell, we normalized the total amount of vRNA to the percentage of Core-expressing cells, as measured by flow cytometry (compare Fig. 2A). Intracellular vRNA levels were initially high, reflecting the effective electroporation of RNA genomes, and increased slightly with a plateau at 48 hpe (Fig. 2E). More importantly, extracellular vRNA levels, reflecting released viral genomes, increased continuously over time, indicating assembly and release of viral particles for all of the tested variants (Fig. 2F). Notably, the level of Jc1-E1(A4) RNA was found to have increased approximately 10-fold in the supernatants compared to the fluorescently labeled variants, which might reflect reduced packaging efficiency due to the increased size of the chromophore-encoding viral genomes. To exclude the possibility that the fluorescently labeled E1 protein was defective in assembling the viral envelope and that the composition of released viral particles differed from that of unlabeled particles, we next employed biochemical assays.

E1 and E2 form heterodimers in the viral envelope (45, 46), and this process might be impeded by fusion of E1 with mCherry. Using lysates from cells electroporated with Jc1-Flag-E2 (33) or Jc1-E1(A4)-mCherry/Flag-E2 (see Fig. 1A) expressing a Flag-tagged E2 glycoprotein, we performed immunoprecipitation (IP) against Flag. As expected, E1 precipitated with Flag-E2 and, more importantly, the interaction of E2 with E1 was not disrupted by the mCherry tag (Fig. 2G).

HCV is a so-called lipo-viral particle (LVP), a condition that results in a buoyant density profile characteristic of released viral particles (33, 47). To investigate whether viral particles of Jc1-E1(A4)-mCherry are assembled and released similarly to wild-type (WT) HCV Jc1 particles, we fractionated supernatants from Jc1-E1(A4)- and Jc1-E1(A4)-mCherry-expressing cells and analyzed these fractions for the presence of E2, E1(A4), and Core. The structural viral proteins of Jc1-E1(A4) as well as of Jc1-E1(A4)-mCherry were present in the same fractions at levels between 1.07 and 1.17 g/ml and peaked at densities of 1.13 g/ml [Jc1-E1(A4)] and 1.14 g/ml [Jc-E1(A4)-mCherry] (Fig. 2H), which were similar to the levels seen with vRNA genomes (Fig. 2I). Importantly, this pattern coincided with detection of ApoE, which was most abundant in fractions with levels ranging from 1.08 to 1.16 g/ml (Fig. 2H, lower panel). Hence, although Jc-1E1(A4)-mCherry might have had a slightly higher density, presumably due

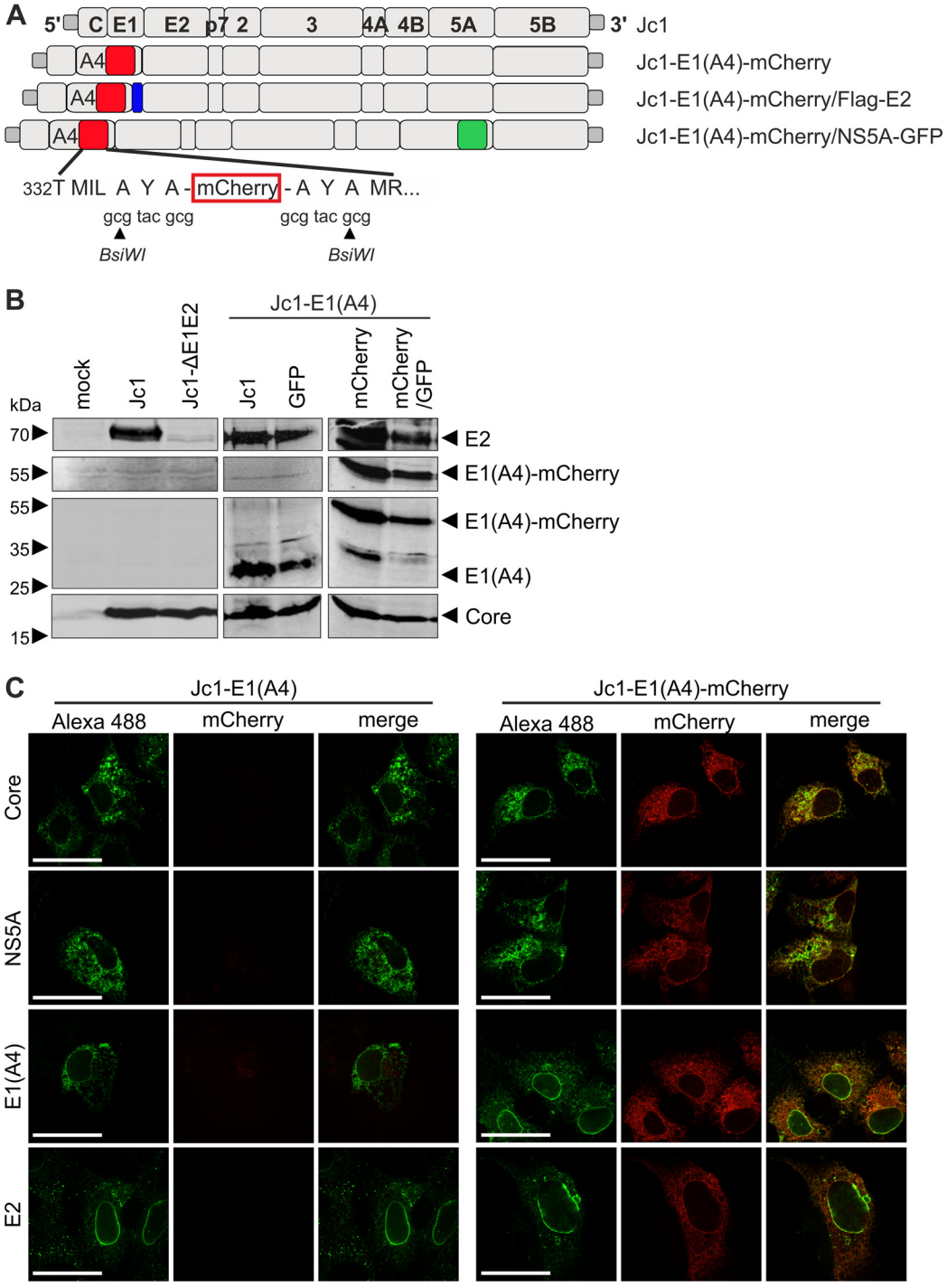

FIG 1 Construction of E1-mCherry-labeled HCV Jc1 variants. (A) Schematic representation of HCV-Jc1 genomes generated in this study. The HCV-Jc1 genome is depicted at the top for reference. We modified this backbone to express mCherry within the E1 glycoprotein with or without NS5A-GFP, Flag-E2, or the A4 epitope in E1 for recognition by the anti-E1 A4 antibody (see Materials and Methods for details). Green box, GFP; red box, mCherry; blue box, Flag tag. (B) Huh7.5 cells were lysed at 48 h postelectroporation (hpe) with RNA of Jc1-WT or Jc1-ΔE1/E2 or variants of Jc1-E1(A4), and expression of viral proteins was analyzed by Western blotting. Blots representative of results of at least three individual experiments are shown. (C) Confocal images of HCV-Jc1-E1(A4) and HCV-Jc1-E1(A4)-mCherry Huh7.5 cells electroporated at 48 hpe show subcellular localization of viral proteins visualized by immunofluorescence staining and localization of E1-mCherry. Scale bar, 35 μm.

to the mCherry tag, the viral structural proteins appeared in the same density fractions as the vRNA genomes and with the specific density of infectious cell culture-produced HCV (HCVcc) particles (47). This strongly indicates authentic assembly and release of HCV Jc1-E1(A4)-mCherry in a manner comparable to that seen with untagged HCV Jc1-E1(A4).

Taking the results together, the mCherry tag within E1 did not interfere with stable expression or intracellular localization of E1

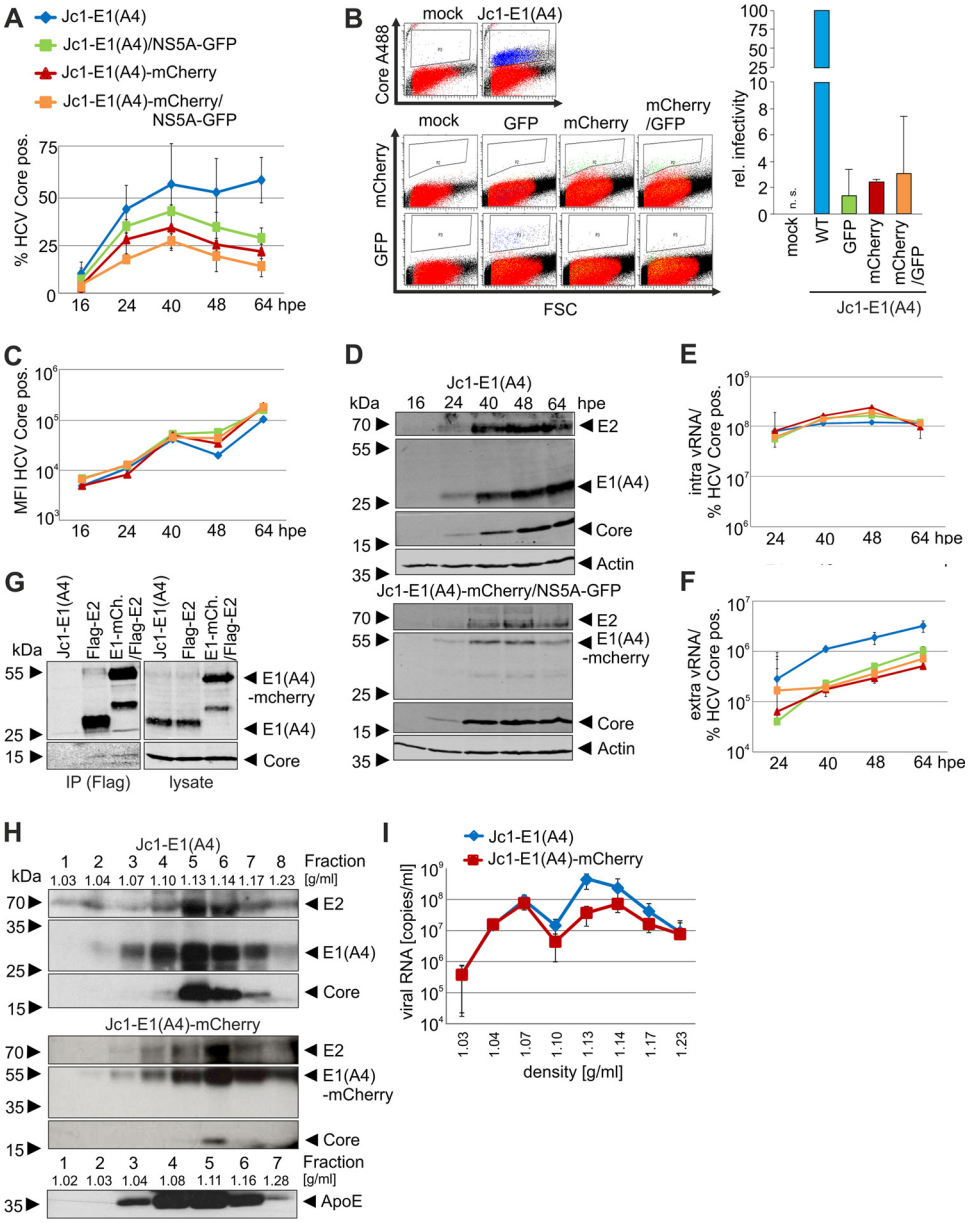

FIG 2 Characteristics of Jc1-E1(A4)-mCherry variants. (A) Huh7.5 cells were electroporated with RNA of Jc1-E1(A4), Jc1-E1(A4)/NS5A-GFP, Jc1-E1(A4)-mCherry, or Jc1-E1(A4)-mCherry/NS5A-GFP and harvested at the indicated time points to be fixed, permeabilized, and stained for HCV Core before analysis by flow cytometry. The percentage of Core-positive (Core pos.) cells over a time course of 64 hpe is shown. Error bars indicate standard deviations (SD) of results from two individual biological replicates per data point. (B) Huh7.5 cells were electroporated with RNA of the indicated viruses. Supernatants were collected 65 hpe, cleared by centrifugation and filtration, and concentrated by ultracentrifugation before they were used for infection of naive Huh7.5 cells. Infected cells were harvested 72 h postinfection (hpi) and stained for expression of intracellular Core in the case of mock-infected and Jc1-E1(A4)-infected cells, and MFI was analyzed by flow cytometry. The percentage of infected cells was calculated relative (rel.) to the number of Core-positive cells electroporated with the indicated RNAs and then normalized to Jc1-E1(A4)-infected cells. n.s., no signal. FACS plots are shown to illustrate the shift of cells when they express the corresponding fluorescent viral proteins. (C) The mean fluorescence intensity (MFI) of the HCV Core-positive cell population from the experiment described for panel A over a time course of 64 hpe is shown. (D) Huh7.5 cells electroporated with RNA of HCV Jc1-E1(A4) or HCV Jc1-E1(A4)-mCherry/NS5A-GFP were lysed at the indicated time points, and expression of viral proteins was analyzed by Western blotting. Actin was used as a loading control. Blots representative of results of two individual experiments are shown. (E and F) Intracellular RNA (intra RNA) (E) and RNA from supernatants of Huh7.5 cells electroporated with the indicated HCV RNAs (compare panel A) (extra RNA) (F) were extracted, and qRT-PCR was performed as described in Materials and Methods to quantify the amount of vRNA genomes. The number of genomes was normalized to the percentage of HCV-expressing cells as assessed by Core staining (compare panel A). Error bars indicate SD of results of two individual biological replicates per data point. (G) Huh7.5 cells were electroporated with RNA of Jc1-E1(A4), Jc1-E1(A4)/Flag-E2, or Jc1-E1(A4)-mCherry/Flag-E2 and lysed 48 hpe. Lysates were subjected to immunoprecipitation (IP) using an antibody against Flag and blotted against Core, E1(A4), and E2. Blots representative of results of three individual experiments are shown. (H) Huh7.5 cells were electroporated with RNA of Jc1-E1(A4) or Jc1-E1(A4)-mCherry, and supernatants harvested 72 hpe were subjected to ultracentrifugation and density gradient fractionation. Proteins of the different fractions were separated by SDS-PAGE and analyzed by Western blotting. Blots representative of results of three individual experiments (one experiment included detection of ApoE; see lower panel). (I) Aliquots of the fractions obtained as described for panel E were used for RNA extraction and subsequent qRT-PCR analysis to detect vRNA genomes. Error bars indicate SD of results of three individual experiments.

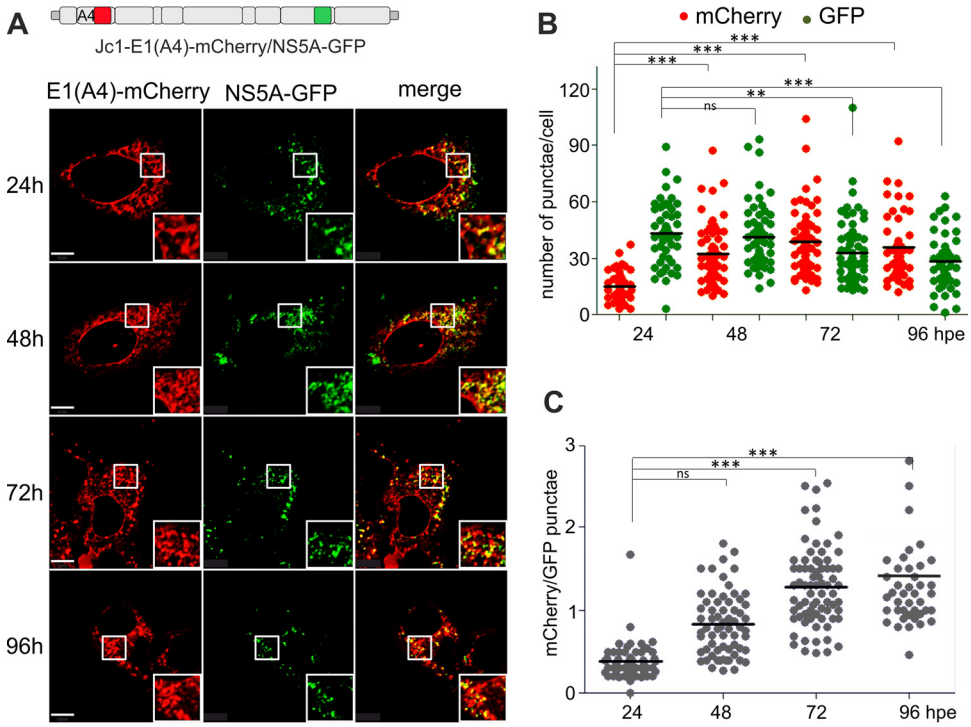

FIG 3 Temporospatial formation of NS5A-GFP replication complexes and E1(A4)-mCherry punctae. Huh7.5 cells were electroporated with RNA of Jc1-E1(A4)-mCherry/NS5A-GFP. (A) A confocal image of living cells showing mCherry and GFP fluorescence was taken every 24 h for up to 96 hpe (see also Movies S1 to S6 in the supplemental material). Representative images from two individual experiments with 22 and 38 analyzed cells, respectively, are shown. Scale bars, 9 μm. White boxes indicate areas of magnification. (B) Cells imaged as described were analyzed for punctae of E1(A4)-mCherry and NS5A-GFP with an arbitrarily chosen maximum threshold of 0.8-μm diameter. Punctae were counted with the spot-counting tool (Volocity). Each dot indicates the number of punctae in one cell, where red dots represent E1(A4)-mCherry punctae and green dots represent NS5A-GFP punctae. (C) Ratios of E1(A4)-mCherry accumulations to NS5A-GFP accumulations were calculated for each cell. Differences between the data in panels B and C were assessed for statistical significance with a one-way ANOVA with posttest. *, $P \leq 0.05$; **, $P \leq 0.01$; ***, $P \leq 0.001$; ns, not significant.

or of the other viral proteins tested. Furthermore, kinetics of viral protein expression and vRNA replication appeared undisturbed by the tag and E1-mCherry interacted with E2. Most importantly, released viral particles tagged with E1-mCherry showed similar growth kinetics and the same biochemical characteristics as WT HCV, demonstrating authentic morphogenesis and secretion of our novel fluorescently labeled Jc1-E1(A4)-mCherry and Jc1-E1(A4)-mCherry/NS5A-GFP variants. Hence, the E1-mCherry-tagged HCV Jc1 variants presented here represent appropriate and unique tools for the study of the dynamics of HCV assembly and release in living cells.

Production of HCV structural protein and replication complexes appears to be temporospatially organized. There is a rapid appearance of replication complexes (RCs) in HCV replicon-expressing Huh7.5 cells visualized by NS5A-GFP, and these RCs can be stable over several hours (48–50). Accordingly, we aimed to characterize the dynamics and formation of NS5A-GFP RCs and E1-mCherry structural protein accumulations, which could represent assembling or assembled viral particles in cells expressing full-length HCV. Jc1-E1(A4)-mCherry/NS5A-GFP-electroporated Huh7.5 cells were imaged over 4 days at the indicated time points starting at 24 hpe, when fluorescence emission from E1-mCherry and NS5A-GFP was detectable (Fig. 3A). As expected, there was rapid formation of NS5A-GFP in RCs (48, 49) and E1-mCherry seemed to accumulate in distinct punctae in addition to the typical ER-associated expression pattern. From the visual inspection of various images (see examples in Fig. 3A), we got the impression of a time-dependent decrease in RCs whereas E1-mCherry punctae seemed to accumulate. For rigorous image quantification, we performed spot counting on multiple cells from independent electroporations with an arbitrary threshold of 0.8 μm as the maximum spot size (Fig. 3B), which is similar to previous analyses (48, 51). At 24 hpe, although E1-mCherry fluorescence was readily detectable, there were only a few punctae in comparison to the number of NS5A-GFP RCs. In contrast, the number of E1-mCherry punctae increased 2.4-fold at 48 hpe compared to the 24 hpe time point and the number of RCs stayed constant (Fig. 3B). At 72 and 96 hpe, the amount of E1-mCherry punctae further increased or remained at the same level, whereas we observed a continuous decline in the number of NS5A-GFP RCs (Fig. 3B). Calculating the ratios of E1-mCherry punctae to NS5A-GFP RCs for each cell over the 96-h observation period revealed a continuous increase, suggesting that formation of RCs commenced quickly after electroporation and slowed down over time while structural protein accumulations in the form of distinct punctae were steadily increasing (Fig. 3C).

Time-dependent increase in interaction of HCV E1-mCherry punctae with the other structural proteins, E2 and Core. The fact that the number of E1-mCherry punctae increased over time suggests that these punctae might represent intracellular assembly sites of HCV particles. Since we expected intracellular assembly sites to recruit the other structural proteins, Core and

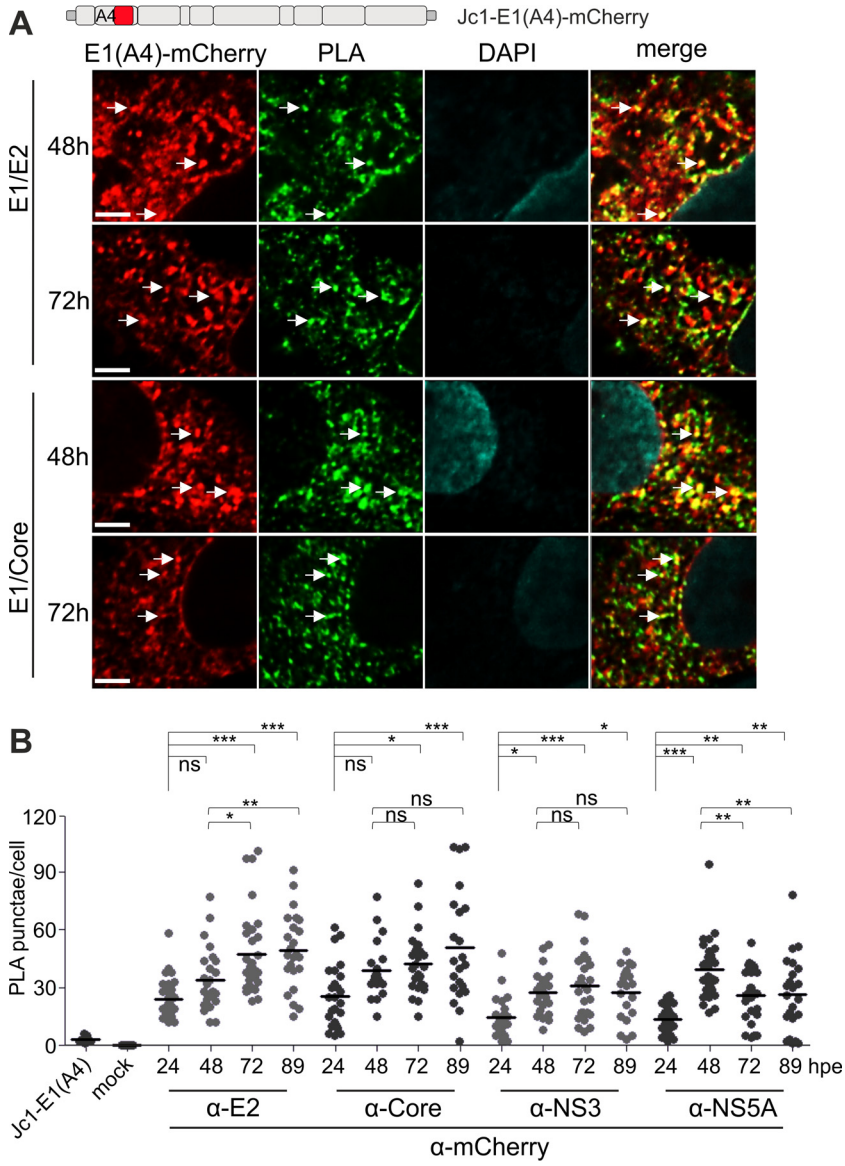

FIG 4 Temporal dynamics of viral protein interactions at E1(A4)-mCherry punctae. Huh7.5 cells were electroporated with RNA of Jc1-E1(A4)-mCherry and fixed at the indicated time points and processed for proximity ligation assay (PLA) with primary antibodies against mCherry and E2 or Core or NS3 or NS5A depending on the interaction analyzed. (A) Representative magnified and cropped images to show areas of PLA-positive samples stained for E1(A4)-mCherry and E2 or E1(A4)-mCherry and Core at 48 hpe and 72 hpe. White arrows show exemplary E1(A4)-mCherry punctae with a positive PLA signal. Scale bar, 3.5 μm. DAPI, 4′,6-diamidino-2-phenylindole. (B) Quantitative analysis of PLA-positive punctae/cell is shown for ≥20 cells per condition using the spot-counting tool (Volocity) with an arbitrarily chosen maximum threshold of 0.8-μm diameter. Differences were assessed for statistical significance with a one-way ANOVA with posttest. *, $P \leq 0.05$; **, $P \leq 0.01$; ***, $P \leq 0.001$; ns, not significant.

E2, we analyzed the interaction of E1-mCherry punctae with E2 and Core and, as controls, NS3 and NS5A. Jc1-E1(A4)-mCherry-electroporated Huh7.5 cells were analyzed over a period of 4 days using proximity ligation assay (PLA) as described previously (18) with E1-mCherry as the primary PLA target and the other viral proteins as putative interaction partners. Quantitative analysis of images such as those shown in Fig. 4A clearly demonstrated that E1-mCherry punctae interacted with structural proteins E2 and Core and that these interactions intensified over time (Fig. 4B). The signals were highly specific, since we did not detect a PLA signal when Jc1-E1(A4)-electroporated Huh7.5 cells were incubated with the same antibodies and PLA reagents (Fig. 4B). In addition, interaction of E1-mCherry with NS3 or NS5A was less pronounced, such that the number of PLA punctae per cell slightly increased from 48 to 72 hpe but dropped again at later time points. We would expect such a result in assuming initial colocalization of E1 and NS5A at the surface of lipid droplets during the formation of assembly sites followed by separation of the two proteins at the onset of viral assembly and release (Fig. 4B). This finding is also in accordance with our observations on formation of punctae of E1-mCherry and NS5A-GFP (Fig. 3B) and live-cell imaging of Jc1-E1(A4)-mCherry/NS5A-GFP-expressing Huh7.5 cells from 24 to 96 hpe (see Movies S1 to S6 in the supplemental material).

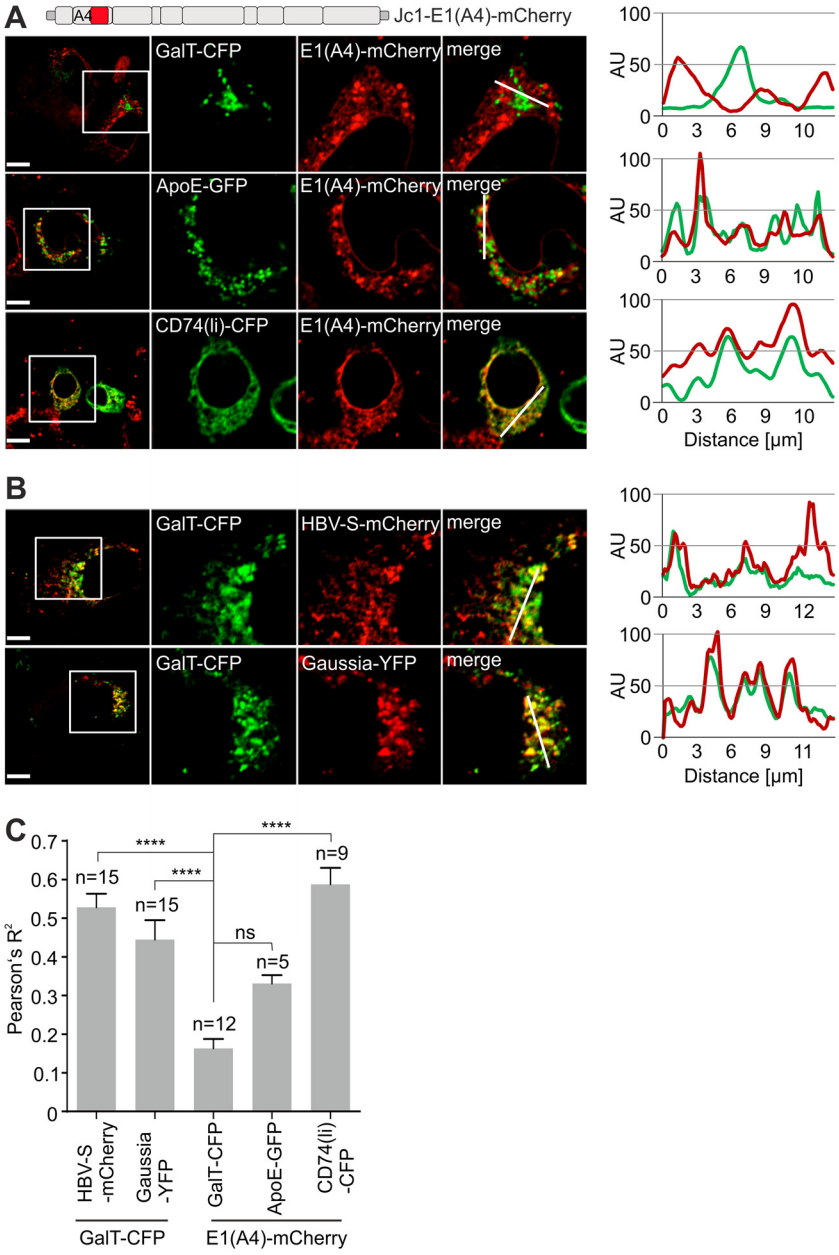

FIG 5 E1(A4)-mCherry punctae do not colocalize with Golgi markers but do colocalize with ER and endosomal markers. (A and B) Living Huh7.5 cells coelectroporated with RNA of Jc1-E1(A4)-mCherry and plasmids expressing GalT-CFP, ApoE-GFP, or CD74(Ii)-CFP (A) or Huh7.5 cells coelectroporated with plasmids encoding GalT-CFP and HBV-S-mCherry or Gaussia-YFP (B) were analyzed by confocal microscopy 56 hpe. (C) Images were merged, and colocalization was analyzed by the use of a fluorescence line profile (white lines in merged images) and by calculation of the Pearson's R^2 value. The number of cells analyzed is indicated above every column. Differences were assessed for statistical significance with a one-way ANOVA with posttest. ns, not significant; ****, $P \leq 0.0001$. Scale bar, 11 μm. The white squares depict the areas that were digitally magnified. The fluorescence intensity in the line profiles is given in arbitrary fluorescence units (AU).

E1-mCherry punctae are not detectable within the Golgi apparatus. E1-mCherry punctae might to some extent represent assembled virions which are ready for release or are in the process of secretion (Fig. 4). Therefore, results of colocalization analyses of E1-mCherry punctae with markers of cellular pathways should be indicative of the HCV secretory route. To investigate this, we first aimed to define the HCV secretory pathway by colocalization studies and coelectroporated Huh7.5 cells with RNA of Jc1-E1(A4)-mCherry and vectors encoding GalT-CFP (Golgi apparatus) or ApoE-GFP (lipoprotein trafficking) or CD74(Ii)-CFP (ER and endosomal compartment) and analyzed these cells 56 hpe by confocal microscopy. As expected, the bulk of E1-mCherry protein colocalized with the CD74 chaperone, which is located in the ER and endosomes/multivesicular bodies (MVBs), and with ApoE (Fig. 5A). However, E1-mCherry punctae did not colocalize with the GalT Golgi marker (see line profiles in Fig. 5A). To exclude the possibility that the electroporation procedure might interfere with Golgi function or that there is an as-yet-unknown Golgi defect in

the Huh7.5 cells used, we coelectroporated vectors expressing hepatitis B virus (HBV)-S–mCherry or Gaussia luciferase-YFP, each of which is known to be secreted through the Golgi apparatus (52, 53), together with the GalT-CFP fusion. Both proteins showed strong colocalization with GalT-CFP as evident from the line profiles (Fig. 5B), suggesting the presence of intact Golgi function in Huh7.5 cells. In addition, the quantitative analyses of Pearson's colocalization coefficient from multiple cells confirmed the absence of E1-mCherry detection within the Golgi apparatus (GalT-CFP) and quantitatively corroborated colocalization with CD74 and ApoE (Fig. 5C).

HCV glycoproteins have a high-mannose glycan structure. During secretion, Golgi-residing enzymes process glycoproteins and modify asparagine-linked mannose-rich oligosaccharides into complex glycans. Complex glycans are resistant to treatment with the EndoH endoglycosidase but are cleaved by peptide:*N*-glycosidase F (PNGaseF). By implication, the EndoH sensitivity of glycoproteins indicates the presence of high-mannose glycans and the absence of glycoprotein modification by Golgi-residing enzymes (54). We therefore assessed the EndoH sensitivity of cell- and virus-associated HCV E1 and E2 glycoproteins.

First, we verified proper processing of a Golgi-secreted glycoprotein in Huh7.5 cells. Supernatants from cells transfected to express the HBV-S glycoprotein were harvested, left untreated, digested with PNGaseF or EndoH, and subjected to WB analysis (Fig. 6A). As expected, HBV-S, which is secreted through the Golgi apparatus and is therefore glycosylated in a complex manner, was resistant to EndoH and could be deglycosylated only by PNGaseF (Fig. 6A) (53).

We repeated the same experiment with lysates from cells that were electroporated with HCV Jc1-E1(A4). In contrast to secreted HBV-S, cell-associated HCV E1 and E2 were sensitive to EndoH and PNGaseF (Fig. 6B), and we observed deglycosylation of E1 and E2 in a dose-dependent manner for both enzymes (Fig. 6C).

It is possible that Golgi enzymes modify only a small fraction of E1 and E2 and that this fraction is incorporated into released viral particles. Hence, we harvested the supernatants of HCV Jc1(A4)-expressing Huh7.5 cells which were concentrated by ultracentrifugation and fractionated by the use of an iodixanol gradient prior to treatment with EndoH and PNGaseF (Fig. 6D). Of note, E1 and E2 in fraction 3 displayed a partly EndoH-resistant phenotype. However, judged on the basis of the absence of detectable HCV Core, this fraction does not appear to contain significant amounts of assembled particles. In contrast, E1 and E2 associated with the vast majority of assembled virus particles in fraction 5 (as well as in all other fractions) were fully sensitive to EndoH digestion (Fig. 6D). In conclusion, the majority of the HCV E1 and E2 glycoproteins associated with assembled and released viral particles had not been modified by Golgi-residing enzymes and exhibited a high-mannose glycan structure.

HCV E1-mCherry punctae traffic with Rab9A-positive compartments. Since E1-mCherry punctae were not associated with Golgi structures but partly colocalized with ApoE and CD74 (Fig. 5), we aimed to identify intracellular trafficking compartments potentially involved in HCV release. Involvement of the endosomal compartment in HCV Core trafficking was previously postulated (23, 55–57). Hence, we coelectroporated Huh7.5 cells with RNA of HCV Jc1-E1(A4)-mCherry and vectors encoding Rab7A-CFP or Rab9A-CFP and VSV-G–GFP as a control glycoprotein that is known to traffic through the Golgi apparatus during mat-

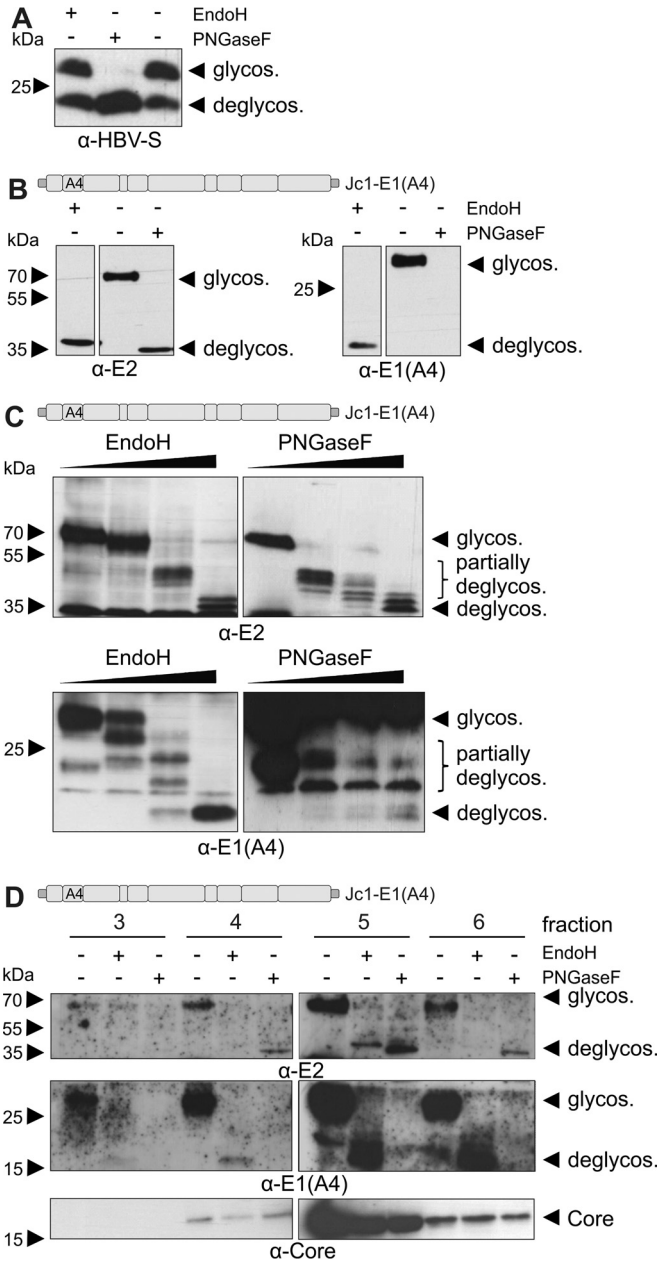

FIG 6 Glycoproteins on released HCV particles are EndoH sensitive. Huh7.5 cells were transfected with a plasmid encoding HBV-S (A) or electroporated with RNA of Jc1-E1(A4) (B to D). (A) Western blot of supernatants from HBV-S-expressing cells at 72 h posttransfection that were concentrated by ultracentrifugation and treated with EndoH (0.5 μl) and PNGaseF (0.1 μl) as indicated. glycos., glycosylation; deglycos., deglycosylation. (B and C) Lysates from Jc1-E1(A4)-electroporated Huh7.5 cells were generated at 72 hpe and digested with 0.5 μl EndoH and PNGaseF (B) or with increasing doses of EndoH (0 μl, 0.01 μl, 0.05 μl, and 0.5 μl) or PNGaseF (0 μl, 0.01 μl, 0.025 μl, and 0.1 μl) (C) to assess dose dependency by Western blotting. (D) Supernatants from Jc1-E1(A4)-electroporated Huh7.5 cells were collected at 72 hpe, concentrated, and density gradient fractionated as described in Materials and Methods. The individual fractions were digested with 0.5 μl EndoH and 0.1 μl PNGaseF before Western blotting. The densities of the fractions depicted were 1.06 g/ml (lanes 3), 1.08 g/ml (lanes 4), 1.12 g/ml (lanes 5), and 1.16 g/ml (lanes 6). Data represent results of one experiment representative of at least three independent biological replicates.

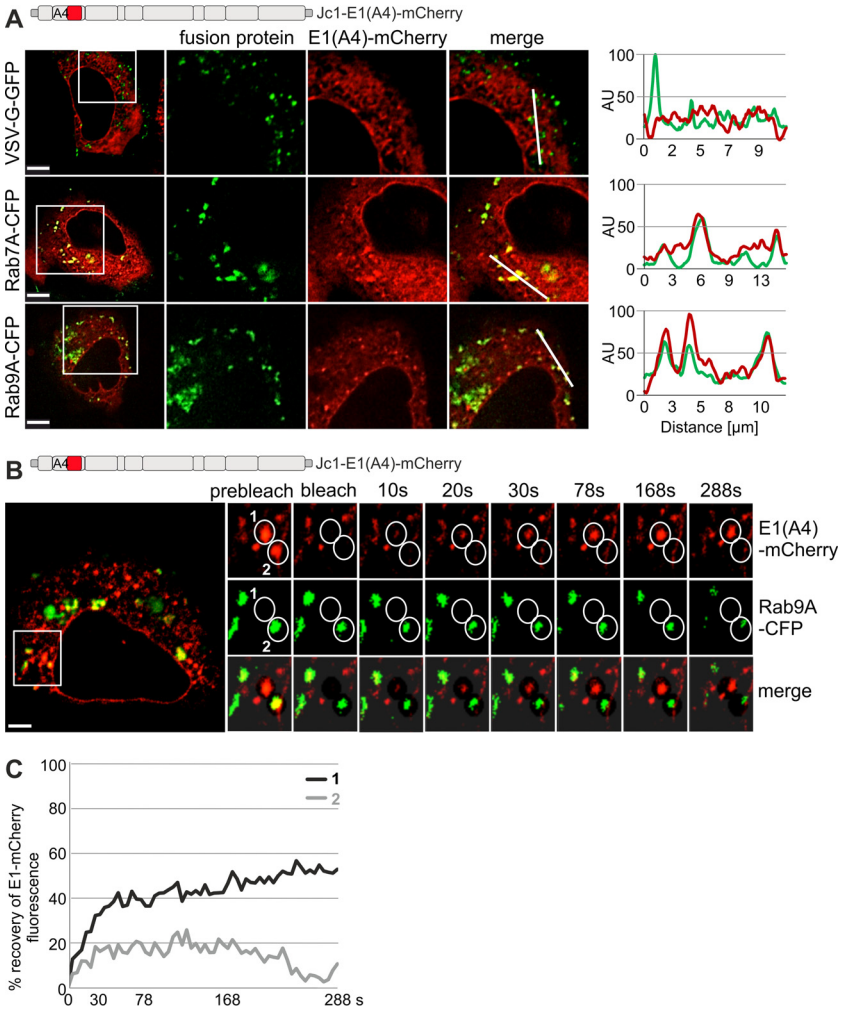

FIG 7 E1(A4)-mCherry punctae traffic with Rab9A-positive compartments. (A) Living Huh7.5 cells coelectroporated with RNA of Jc1-E1(A4)-mCherry and plasmids encoding VSV-G–GFP, Rab7A-CFP, and Rab9A-CFP were analyzed using by confocal microscopy 48 hpe. Scale bars, 11 μm. The fluorescence intensity in the line profiles is given in arbitrary fluorescence units (AU). Green lines represent GFP/CFP fluorescence; red lines represent E1(A4)-mCherry fluorescence. (B) Living Huh7.5 cells coelectroporated with RNA of Jc1-E1(A4)-mCherry and a plasmid encoding Rab9A-CFP were used for fluorescence recovery after photobleaching (FRAP) analysis 53 hpe. Scale bar, 11 μm. White circles indicate areas that were photobleached (circles 1 and 2), and fluorescence recovery was imaged over a time period of 288 s (compare Movie S8 in the supplemental material). Images representative of the indicated time points are shown. (C) The fluorescence intensity profile of the depicted areas was assessed over time and normalized to the fluorescence intensity in the bleached area before FRAP (set as 100%). The black line represents fluorescence recovery of circle 1; the dark gray line represents fluorescence recovery of circle 2. Multiple cells and punctae with E1(A4)-mCherry and/or Rab9A-CFP fluorescence were analyzed with FRAP, and results were similar to those seen with the representative sequence shown here (also compare Movie S8 in the supplemental material).

uration (58). Rab7A and Rab9A are cellular proteins that have roles in late endosomal trafficking (59). Colocalization of E1-mCherry and the indicated proteins was analyzed 48 hpe by line profiling. Consistent with our previous results (Fig. 5), we did not observe any colocalization of E1-mCherry with VSV-G–GFP (Fig. 7A, top row). In contrast, few E1-mCherry punctae appeared to colocalize with Rab7A-CFP and Rab9A-CFP (Fig. 7A, mid and bottom rows).

Assembling HCV particles might be connected to sites of viral protein translation and trafficking, whereas assembled particles are most likely present in membrane-enclosed transport compartments. We first explored the nature of intracellular E1-mCherry punctae with fluorescence recovery after photobleaching (FRAP) and indeed confirmed the presence of different types of E1-mCherry punctae that either stayed bleached or could recover fluorescence to some extent (see Movie S7 in the supplemental material). This supports our hypothesis of the presence of assembled viral particles within membrane-enclosed compartments. The endosomal compartment and, more specifically, Rab9A-positive vesicles could be part of such an intracellular trafficking pathway. Hence, we repeated FRAP with Huh7.5 cells coelectroporated with HCV Jc1-E1(A4)-mCherry RNA and a vector encoding Rab9A-CFP (Fig. 7B; see also Movie S8 in the supplemental material). When we specifically bleached a Rab9A-negative E1-mCherry punctum, E1-mCherry fluorescence recovered to nearly 60% within 300 s (Fig. 7C). In contrast, the E1-mCherry fluorescence of a punctum positive for Rab9A-CFP did not recover (Fig. 7B and C).

Taken together, these data indicate that intracellular trafficking of E1-mCherry, which might be associated with assembled

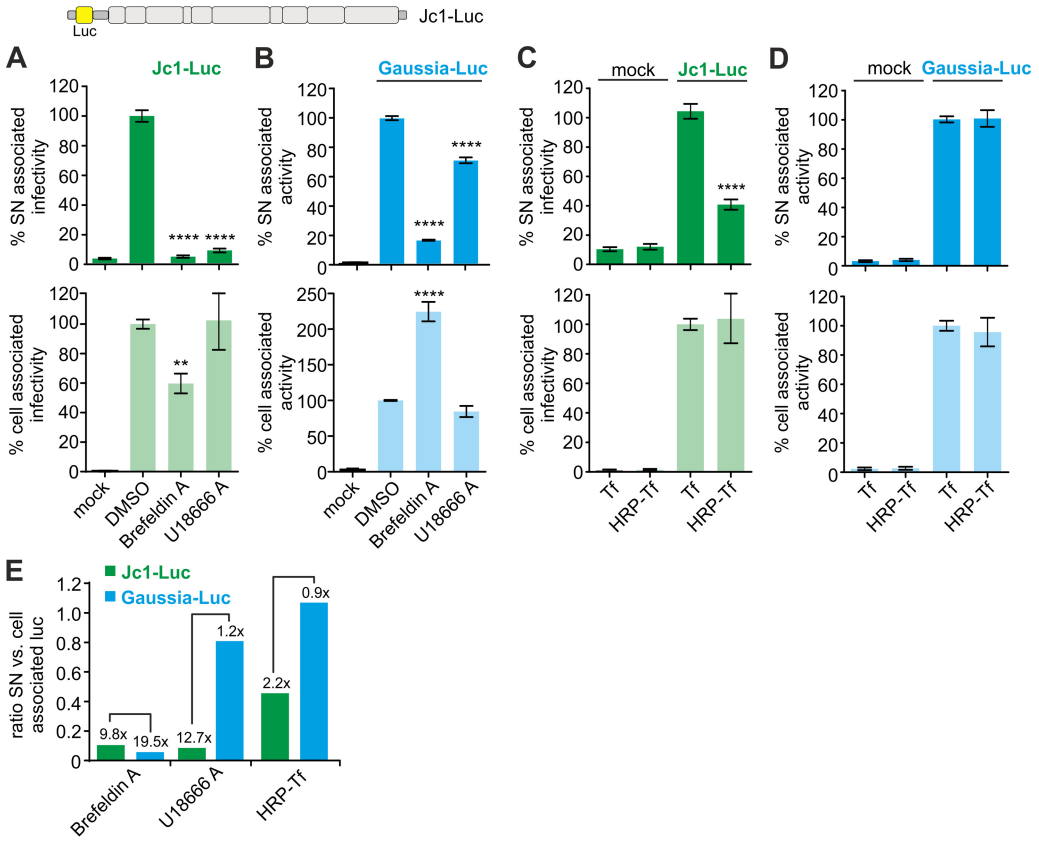

FIG 8 HCV but not Gaussia luciferase (Luc) release is suppressed by inhibition of the endosomal compartment. (A) Huh7.5 cells were electroporated with HCV Jc1-luc RNA. At 40 hpe, the medium was changed and fresh medium containing the indicated drugs was added. At an additional 8 h later, supernatants (SN) were harvested and sucrose gradient centrifuged in order to remove the drugs and purify newly produced virus. Pellets were resuspended and used to inoculate uninfected Huh7.5 cells. At 72 h later, cells were lysed and luciferase activity (hence, viral infection) was quantified. The graph shows mean values and standard errors of the means (SEM) of results of four to nine independent electroporation experiments. As shown in the lower panel, we measured Jc1-luc activity in lysates of the producer cells. (B) Same experimental setting as described for panel A; however, Huh7.5 cells were electroporated with a Gaussia luciferase reporter construct. At 8 h later, supernatants were taken and secreted Gaussia luciferase was quantified. The graph shows mean values and SEM of results from six independent electroporations. (C) Huh7.5 cells were electroporated with HCV JC1-luc RNA. At 40 hpe, cells were starved and either transferrin (Tf) or transferrin conjugated with horseradish peroxidase (HRP-Tf) was added and allowed to internalize for 2 h. Subsequently, endosomes were chemically fixed inside living cells as described in Materials and Methods and previously (42, 43). Next, the medium was changed and cells were allowed to produce virus for additional 8 h. Supernatants were taken and sucrose gradient purified and used to inoculate uninfected Huh7.5 cells in order to quantify the amount of released virus. Furthermore, Jc1-luc activity was quantified by measurement of luciferase activity in the producer cells (lower panel). Mean values and SEM from 15 independent electroporation experiments are depicted. (D) Same experimental design as that described for panel C except that a Gaussia luciferase reporter construct was electroporated. Furthermore, the amount of released Gaussia luc was directly quantified in the supernatants. Mean values and SEM from seven independent experiments are shown. Differences were assessed for statistical significance with a one-way ANOVA with posttest. **, $P \leq 0.01$; ****, $P \leq 0.0001$.

HCV particles, involves the endosomal compartment and, more specifically, Rab9A-positive vesicles.

Inhibition of the early endosomal pathway suppresses HCV release. Our data indicate that HCV release involves the endosomal compartment. To assess this in a quantitative manner, we used U18666A, which inhibits intracellular movement of endosomes through blocking cholesterol *de novo* synthesis and transport of LDL-derived cholesterol (60, 61). Of note, while prolonged incubation with U18666A for 48 h or longer suppresses HCV RNA replication (62), shorter incubation periods have no such effect and were previously used to inhibit HCV release (55). We therefore electroporated Huh7.5 cells with RNA of HCV Jc1-luc (32) and incubated the cells with U18666A at 48 hpe for 8 h. For a positive control, we included brefeldin A, which completely blocks vesicular protein transport from the ER (63, 64). We then cleared HCV-luc-containing supernatants by sucrose centrifugation and used them to infect native Huh7.5 cells to quantify infectious virus particle release by luciferase activity in cell lysates (Fig. 8A). To directly compare the effects of the inhibitor on a cargo that is released via secretion through the Golgi apparatus, we used Huh7.5 cells, which were electroporated with a plasmid encoding Gaussia luciferase (35, 52). This approach directly allows assessment of the efficiency of Gaussia secretion by measurement of luciferase activity in the supernatant (Fig. 8B). Addition of brefeldin A completely blocked HCV and Gaussia release (Fig. 8A and B), and this effect was reversible (data not shown). However, as reported before (65), we also noticed that brefeldin A had an inhibiting effect on intracellular levels of HCV-associated luciferase activity and hence most likely on viral RNA replication (Fig. 8A, lower panel). In contrast, U18666A completely inhibited HCV release (Fig. 8A) but affected Gaussia secretion only marginally (Fig. 8B). This effect was specific for release, since the concentra-

tion of U18666A used here (25 μM) had no inhibitory effect on intracellular virus production (Fig. 8A, lower panel).

In general, inhibitors, including U18666A, might have nonspecific side effects. Hence, we applied an independent technique for specific inhibition of the early endosomal pathway based on biochemical fixation of endosomes (42, 43). Huh7.5 cells electroporated with RNA of HCV Jc1-luc or transfected to express Gaussia luciferase were fed with horseradish peroxidase (HRP) coupled to transferrin (Tf), which is taken up into the early endosomal pathway. Addition of the HRP substrate DAB (3,3′-diaminobenzidine) chemically fixes endosomes within living cells and thus inactivates the endosomal pathway without damaging the cells. After inactivation of endosomes, we allowed the cells to produce virus/Gaussia luciferase in the supernatant for 8 h and then measured supernatant-associated infectivity with the HCV Jc1-luc strain (Fig. 8C) or Gaussia luciferase activity (Fig. 8D). Inactivation of endosomes strongly suppressed HCV release in comparison to control cells that were treated identically but fed with Tf instead of HRP-Tf (Fig. 8D). Strikingly, the release of Gaussia luciferase was not affected by fixation of early endosomes (Fig. 8D) and the procedure had no negative effects on intracellular levels of HCV or Gaussia (Fig. 8C and D, lower panels). From the comparative analysis of HCV release versus Gaussia release (Fig. 8E), we conclude that the endosomal pathway is integral to HCV release and that secretion of viral particles differs from the canonical secretory route.

DISCUSSION

Here, we established and exploited fluorescently labeled HCV genomes to study intracellular viral trafficking and the dynamics of structural and nonstructural protein expression. HCV genomes or replicons containing a GFP tag within NS5A were described previously and were successfully used to analyze intracellular movement of the replication complex and to investigate HCV superinfection (31, 48, 50, 66). In contrast to this, our novel HCV Jc1 variants containing mCherry within E1 allowed tracking of intracellular distribution of a structural protein and its movement and are alternatives to the HCV genomes with a tetracysteine tag in Core (28, 51). Core is posttranslationally processed and is targeted to the ER through its C terminus (17, 67). Furthermore, it contains *cis*-active elements that are important for regulation and initiation of polyprotein translation (68) and plays a crucial role in assembly and release (8, 17, 69). We therefore chose to introduce the tag into one of the envelope proteins of HCV. Since E2 mediates attachment to cellular receptors and shields E1 in a heteromeric complex (1, 70), we inserted mCherry between the C-terminal glycosylation site and the N terminus of the transmembrane domain of E1. While the tag unfortunately reduced infectivity (Fig. 2B), Jc1-E1(A4)-mCherry and Jc1-E1(A4)-mCherry/NS5A-GFP showed normal levels of polyprotein expression and processing. Furthermore, comprehensive biochemical analyses demonstrated release of HCV particles from the fluorescently labeled genomes with a level of buoyant density similar to that seen with untagged HCV Jc1 (47) and in conjunction with apolipoprotein (21). Taking the results together, apart from the reduced infectivity, most likely due to structural alterations of the envelope glycoprotein complex, our novel E1-mCherry-tagged HCV genomes show properties comparable to those of WT HCV and hence represent unique and valuable tools to investigate viral morphogenesis, assembly, budding, and egress.

We found temporospatial regulation of structural E1-mCherry and nonstructural NS5A-GFP expression. NS5A was rapidly expressed and localized to punctae most likely representing RCs (48–50). In contrast, E1-mCherry localizations were initially rather dispersed and then accumulated in punctae over the 4-day observation period (Fig. 3; see also Movies S1 to S6 in the supplemental material). Dynamic formation of NS5A RCs and punctae containing structural protein Core has been reported before, and those results are in agreement with our data (28, 48, 50, 51). However, previous studies did not assess formation dynamics over such a long period and did not have the opportunity to monitor the kinetics of E1 and NS5A simultaneously, such as is now feasible with our double-labeled genome. Furthermore, using PLA in conjunction with localization microscopy allowed specific analysis of the time-dependent interaction of HCV proteins within the E1-mCherry punctae (Fig. 4). The temporal increase in levels of E1-mCherry punctae interacting with the other envelope glycoprotein, E2, as well as with the Core capsid protein, strongly supports the identification of E1-mCherry punctae as sites of ongoing HCV assembly or assembled virions. In addition, E1-mCherry punctae transiently interacted with NS proteins (NS3 and NS5A) at 48 hpe and levels of NS5A-GFP RCs decreased from 48 to 96 hpe (Fig. 3). In conclusion, viral replication and translation appear to be initiated rapidly after delivery of viral RNA into the cytoplasm followed by a continuous increase in structural protein interactions, possibly resembling the formation of viral particles. In parallel, levels of RCs continuously decrease, which could reflect a shutdown of vRNA replication and viral protein translation (49).

Conceivably, detection of E1-mCherry punctae at later time points is indicative of the presence of intracellular transport pathways exploited by viral particles. Analyses of cells from 56 to 72 hpe revealed that the E1-mCherry punctae were part of the endosomal compartment and did not carry Golgi markers or colocalize with Golgi-secreted proteins (Fig. 5 and 7). Others have reported trafficking of HCV Core in endosomal compartments (55); however, it was not clear if this proportion of Core is indicative of the presence of assembled virions or of Core protein accumulations alone. Glenn Randall's group performed nonquantitative colocalization analysis, and even though their results look very similar to ours, their results were interpreted in a different way, arguing for a small subproportion of structural protein trafficking through the Golgi structure (28). We have to acknowledge that the presence of such markers is often ambiguous and semiquantitative and gives room for various interpretations. Therefore, we used inhibitors targeting cellular transport pathways and performed biochemical characterization of released HCV particles. Brefeldin A completely blocked the release of infectious particles, which is not surprising, since brefeldin A is a broad-spectrum inhibitor and disrupts trafficking from the ER to the Golgi apparatus to the endosomal compartment and vesicle formation at the plasma membrane (63, 64) as well as HCV RNA replication (71). In contrast, HCV release was suppressed by U18666A, an inhibitor of endosomal trafficking (60), and in an independent experimental setting in which we biochemically fixed early endosomes within HCV-infected Huh7.5 cells. In sum, the different independent lines of evidence presented here support the conclusion that intracellular vesicles containing assembled HCV are part of the endosomal compartment. This is in agreement with another study showing Core trafficking in endosomes (55) and is corroborated by reports demonstrating the involvement of key components of

the endosomal machinery consisting of ESCRT-III, Vps4, TIP47, and Rab9A in HCV production and release (72–75).

Intriguingly, EndoH cleaves glycans of E1 and E2 envelope glycoproteins present in the vast majority of released viral particles (Fig. 6). This demonstrates that the bulk of E1 and E2 is not processed by Golgi-residing enzymes during release and gives rise to the issue of whether assembled HCV is secreted through the Golgi apparatus. Here we propose a noncanonical secretory route for the majority of assembled HCV particles. We base this hypothesis on three lines of evidence: (i) HCV E1-mCherry punctae do not colocalize with Golgi markers; (ii) inhibition of the endosomal compartment specifically inhibits HCV egress but not release of the Golgi-secreted Gaussia luciferase; and (iii) glycoproteins on released HCV particles are sensitive to EndoH.

Our model is not at odds with studies postulating an important role of the Golgi apparatus in HCV release (27, 28, 76). It is entirely conceivable that Golgi-derived factors or Golgi components are important for assembly and/or participate in the release of assembled particles. However, this does not necessarily imply release of assembled virus via the canonical Golgi-mediated secretory route.

Our data are also in accordance with the work of Dubuisson and coworkers (46). In that study, they observed, similarly to our results, that the bulk of E1 glycoprotein in the whole supernatant of cell culture-produced HCV (HCVcc) was EndoH sensitive and that E2 was partly resistant. In line with their results, our data show that a fraction of E1 and E2 was EndoH resistant (density of 1.06 to 1.08 g/ml) (fraction 3; compare Fig. 6D). Although this fraction might resemble only the minority of assembled and released particles, based on the small amounts of glycoprotein as well as Core, it is well known that particles of this density are highly infectious (47). In conclusion, despite the observation that an alternative route is taken by the bulk of HCV particles, the canonical secretory pathway might still give rise to infectious HCV progeny to some degree. The use of a noncanonical pathway by HCV is also compatible with the finding by the Dubuisson group showing that glycoproteins incorporated into HCV pseudoparticles (HCVpp) are EndoH resistant (46). Of note, HCVpp are human immunodeficiency virus type 1 (HIV-1) particles produced from 293T cells which incorporate HCV envelope proteins (77). HCVpps are assembled at the plasma membrane, whereas HCV virions are assembled at the ER close to lipid droplets (LDs) (8, 13). Thus, it is tempting to speculate that the cellular localization of particle assembly determines whether E1 and E2 proteins are modified by Golgi enzymes. Most likely, HCVcc particles incorporate glycoproteins at the ER close to LDs before Golgi passage, whereas HCVpp particles need to incorporate E1 and E2 at the plasma membrane posttrafficking through the Golgi apparatus.

One key unresolved issue remains regarding the exact identity of the noncanonical secretory route taken by HCV. The most provocative hypothesis would be the presence of a not-yet-discovered secretory route bypassing the Golgi apparatus and allowing direct secretion of proteins from the ER and ER-convoluted membranes to the plasma membrane. Such a mechanism is possible, given the fact that Golgi bypass has been described in the literature before (78). Furthermore, rotaviruses are known to bypass the Golgi apparatus during assembly and release, although the mechanisms are poorly understood and the biology of rotaviruses strongly differs from that of HCV (79). Other possible explanations for the phenotypes that we observed are virus-induced alterations of the Golgi complex, including its dispersion, as previously proposed (23, 27), and classical secretion without processing of the HCV glycoproteins by Golgi-residing enzymes due to their putative inaccessibility when they are associated with lipids (33). Given the findings that a proportion of HCV glycoproteins indeed carries complex glycans (46) (Fig. 6D) and that Golgi function is essential for cellular survival, complete Golgi dispersion seems unlikely and the differential levels of egress of HCV versus Golgi-secreted Gaussia luciferase (Fig. 8) indeed argue for an alternative pathway of release.

In sum, this study established HCV viral genomes encoding fluorescently labeled viral proteins, which were exploited to characterize the pathway of HCV release. We discovered a noncanonical and as-yet-unknown route of HCV secretion from Huh7.5 cells involving the endosomal pathway. In the future, it will be important and highly relevant to further characterize this secretory pathway and delineate whether it is induced by HCV to initiate release or if it is an intrinsic property of the cell.

ACKNOWLEDGMENTS

We thank Ulrike Protzer, Gerhard Jahn, and Thomas Iftner for constant support and encouragement. Most importantly, this work would have never been possible without the generous gift of many essential reagents contributed by various researchers. We especially thank Ralf Bartenschlager, Charles Rice, Takashi Wakita, Glenn Randall, Harry Greenberg, Franck Perez, Andrea Musacchio, Philippe Bastiaens, Dieter Glebe, and Genentech for their kind help (see Materials and Methods). Furthermore, we acknowledge Gabrielle Vieyres and Thomas Pietschmann for fruitful and helpful discussions and critical readings of the manuscript.

FUNDING INFORMATION

This study was funded by institutional support to M.S. from the Helmholtz Center Munich, the Heinrich Pette Institute Hamburg, and the University Hospital Tübingen.

REFERENCES

1. **Moradpour D, Penin F, Rice CM.** 2007. Replication of hepatitis C virus. Nat Rev Microbiol **5:**453–463. http://dx.doi.org/10.1038/nrmicro1645.
2. **Gouttenoire J, Penin F, Moradpour D.** 2010. Hepatitis C virus nonstructural protein 4B: a journey into unexplored territory. Rev Med Virol **20:**117–129. http://dx.doi.org/10.1002/rmv.640.
3. **Romero-Brey I, Merz A, Chiramel A, Lee JY, Chlanda P, Haselman U, Santarella-Mellwig R, Habermann A, Hoppe S, Kallis S, Walther P, Antony C, Krijnse-Locker J, Bartenschlager R.** 2012. Three-dimensional architecture and biogenesis of membrane structures associated with hepatitis C virus replication. PLoS Pathog **8:**e1003056. http://dx.doi.org/10.1371/journal.ppat.1003056.
4. **Egger D, Wolk B, Gosert R, Bianchi L, Blum HE, Moradpour D, Bienz K.** 2002. Expression of hepatitis C virus proteins induces distinct membrane alterations including a candidate viral replication complex. J Virol **76:**5974–5984. http://dx.doi.org/10.1128/JVI.76.12.5974-5984.2002.
5. **Gosert R, Egger D, Lohmann V, Bartenschlager R, Blum HE, Bienz K, Moradpour D.** 2003. Identification of the hepatitis C virus RNA replication complex in Huh-7 cells harboring subgenomic replicons. J Virol **77:**5487–5492. http://dx.doi.org/10.1128/JVI.77.9.5487-5492.2003.
6. **Boulant S, Montserret R, Hope RG, Ratinier M, Targett-Adams P, Lavergne JP, Penin F, McLauchlan J.** 2006. Structural determinants that target the hepatitis C virus core protein to lipid droplets. J Biol Chem **281:**22236–22247. http://dx.doi.org/10.1074/jbc.M601031200.
7. **Boulant S, Targett-Adams P, McLauchlan J.** 2007. Disrupting the association of hepatitis C virus core protein with lipid droplets correlates with a loss in production of infectious virus. J Gen Virol **88:**2204–2213. http://dx.doi.org/10.1099/vir.0.82898-0.
8. **Miyanari Y, Atsuzawa K, Usuda N, Watashi K, Hishiki T, Zayas M, Bartenschlager R, Wakita T, Hijikata M, Shimotohno K.** 2007. The lipid

droplet is an important organelle for hepatitis C virus production. Nat Cell Biol **9:**1089–1097. http://dx.doi.org/10.1038/ncb1631.
9. **Cocquerel L, Meunier JC, Pillez A, Wychowski C, Dubuisson J.** 1998. A retention signal necessary and sufficient for endoplasmic reticulum localization maps to the transmembrane domain of hepatitis C virus glycoprotein E2. J Virol **72:**2183–2191.
10. **Cocquerel L, Duvet S, Meunier JC, Pillez A, Cacan R, Wychowski C, Dubuisson J.** 1999. The transmembrane domain of hepatitis C virus glycoprotein E1 is a signal for static retention in the endoplasmic reticulum. J Virol **73:**2641–2649.
11. **Popescu CI, Callens N, Trinel D, Roingeard P, Moradpour D, Descamps V, Duverlie G, Penin F, Heliot L, Rouille Y, Dubuisson J.** 2011. NS2 protein of hepatitis C virus interacts with structural and nonstructural proteins towards virus assembly. PLoS Pathog **7:**e1001278. http://dx.doi.org/10.1371/journal.ppat.1001278.
12. **Stapleford KA, Lindenbach BD.** 2011. Hepatitis C virus NS2 coordinates virus particle assembly through physical interactions with the E1-E2 glycoprotein and NS3-NS4A enzyme complexes. J Virol **85:**1706–1717. http://dx.doi.org/10.1128/JVI.02268-10.
13. **Bartenschlager R, Penin F, Lohmann V, Andre P.** 2011. Assembly of infectious hepatitis C virus particles. Trends Microbiol **19:**95–103. http://dx.doi.org/10.1016/j.tim.2010.11.005.
14. **Oakland TE, Haselton KJ, Randall G.** 2013. EWSR1 binds the hepatitis C virus cis-acting replication element and is required for efficient viral replication. J Virol **87:**6625–6634. http://dx.doi.org/10.1128/JVI.01006-12.
15. **Herker E, Harris C, Hernandez C, Carpentier A, Kaehlcke K, Rosenberg AR, Farese RV, Jr, Ott M.** 2010. Efficient hepatitis C virus particle formation requires diacylglycerol acyltransferase-1. Nat Med **16:**1295–1298. http://dx.doi.org/10.1038/nm.2238.
16. **Camus G, Vogt DA, Kondratowicz AS, Ott M.** 2013. Lipid droplets and viral infections. Methods Cell Biol **116:**167–190. http://dx.doi.org/10.1016/B978-0-12-408051-5.00009-7.
17. **Boson B, Granio O, Bartenschlager R, Cosset FL.** 2011. A concerted action of hepatitis C virus p7 and nonstructural protein 2 regulates core localization at the endoplasmic reticulum and virus assembly. PLoS Pathog **7:**e1002144. http://dx.doi.org/10.1371/journal.ppat.1002144.
18. **Hagen N, Bayer K, Rosch K, Schindler M.** 2014. The intraviral protein interaction network of hepatitis C virus. Mol Cell Proteomics **13:**1676–1689. http://dx.doi.org/10.1074/mcp.M113.036301.
19. **Benga WJ, Krieger SE, Dimitrova M, Zeisel MB, Parnot M, Lupberger J, Hildt E, Luo G, McLauchlan J, Baumert TF, Schuster C.** 2010. Apolipoprotein E interacts with hepatitis C virus nonstructural protein 5A and determines assembly of infectious particles. Hepatology **51:**43–53. http://dx.doi.org/10.1002/hep.23278.
20. **Boyer A, Dumans A, Beaumont E, Etienne L, Roingeard P, Meunier JC.** 2014. The association of hepatitis C virus glycoproteins with apolipoproteins E and B early in assembly is conserved in lipoviral particles. J Biol Chem **289:**18904–18913. http://dx.doi.org/10.1074/jbc.M113.538256.
21. **Lee JY, Acosta EG, Stoeck IK, Long G, Hiet MS, Mueller B, Fackler OT, Kallis S, Bartenschlager R.** 2014. Apolipoprotein E likely contributes to a maturation step of infectious hepatitis C virus particles and interacts with viral envelope glycoproteins. J Virol **88:**12422–12437. http://dx.doi.org/10.1128/JVI.01660-14.
22. **Li X, Jiang H, Qu L, Yao W, Cai H, Chen L, Peng T.** 2014. Hepatocyte nuclear factor 4alpha and downstream secreted phospholipase A2 GXIIB regulate production of infectious hepatitis C virus. J Virol **88:**612–627. http://dx.doi.org/10.1128/JVI.02068-13.
23. **Mankouri J, Walter C, Stewart H, Bentham M, Park WS, Heo WD, Fukuda M, Griffin S, Harris M.** 2016. Release of infectious hepatitis C virus from Huh7 cells occurs via a trans-Golgi network-to-endosome pathway independent of very-low-density lipoprotein secretion. J Virol **90:**7159–7170. http://dx.doi.org/10.1128/JVI.00826-16.
24. **Chambers TJ, Hahn CS, Galler R, Rice CM.** 1990. Flavivirus genome organization, expression, and replication. Annu Rev Microbiol **44:**649–688. http://dx.doi.org/10.1146/annurev.mi.44.100190.003245.
25. **Welsch S, Miller S, Romero-Brey I, Merz A, Bleck CK, Walther P, Fuller SD, Antony C, Krijnse-Locker J, Bartenschlager R.** 2009. Composition and three-dimensional architecture of the dengue virus replication and assembly sites. Cell Host Microbe **5:**365–375. http://dx.doi.org/10.1016/j.chom.2009.03.007.
26. **Weiskircher E, Aligo J, Ning G, Konan KV.** 2009. Bovine viral diarrhea virus NS4B protein is an integral membrane protein associated with Golgi markers and rearranged host membranes. Virol J **6:**185. http://dx.doi.org/10.1186/1743-422X-6-185.
27. **Bishé B, Syed GH, Field SJ, Siddiqui A.** 2012. Role of phosphatidylinositol 4-phosphate (PI4P) and its binding protein GOLPH3 in hepatitis C virus secretion. J Biol Chem **287:**27637–27647. http://dx.doi.org/10.1074/jbc.M112.346569.
28. **Coller KE, Heaton NS, Berger KL, Cooper JD, Saunders JL, Randall G.** 2012. Molecular determinants and dynamics of hepatitis C virus secretion. PLoS Pathog **8:**e1002466. http://dx.doi.org/10.1371/journal.ppat.1002466.
29. **Vieyres G, Dubuisson J, Pietschmann T.** 2014. Incorporation of hepatitis C virus E1 and E2 glycoproteins: the keystones on a peculiar virion. Viruses **6:**1149–1187. http://dx.doi.org/10.3390/v6031149.
30. **Scott KL, Kabbarah O, Liang MC, Ivanova E, Anagnostou V, Wu J, Dhakal S, Wu M, Chen S, Feinberg T, Huang J, Saci A, Widlund HR, Fisher DE, Xiao Y, Rimm DL, Protopopov A, Wong KK, Chin L.** 2009. GOLPH3 modulates mTOR signalling and rapamycin sensitivity in cancer. Nature **459:**1085–1090. http://dx.doi.org/10.1038/nature08109.
31. **Schaller T, Appel N, Koutsoudakis G, Kallis S, Lohmann V, Pietschmann T, Bartenschlager R.** 2007. Analysis of hepatitis C virus superinfection exclusion by using novel fluorochrome gene-tagged viral genomes. J Virol **81:**4591–4603. http://dx.doi.org/10.1128/JVI.02144-06.
32. **Pietschmann T, Kaul A, Koutsoudakis G, Shavinskaya A, Kallis S, Steinmann E, Abid K, Negro F, Dreux M, Cosset FL, Bartenschlager R.** 2006. Construction and characterization of infectious intragenotypic and intergenotypic hepatitis C virus chimeras. Proc Natl Acad Sci U S A **103:**7408–7413. http://dx.doi.org/10.1073/pnas.0504877103.
33. **Merz A, Long G, Hiet MS, Brugger B, Chlanda P, Andre P, Wieland F, Krijnse-Locker J, Bartenschlager R.** 2011. Biochemical and morphological properties of hepatitis C virus particles and determination of their lipidome. J Biol Chem **286:**3018–3032. http://dx.doi.org/10.1074/jbc.M110.175018.
34. **Dubuisson J, Hsu HH, Cheung RC, Greenberg HB, Russell DG, Rice CM.** 1994. Formation and intracellular localization of hepatitis C virus envelope glycoprotein complexes expressed by recombinant vaccinia and Sindbis viruses. J Virol **68:**6147–6160.
35. **Tannous BA, Kim DE, Fernandez JL, Weissleder R, Breakefield XO.** 2005. Codon-optimized Gaussia luciferase cDNA for mammalian gene expression in culture and in vivo. Mol Ther **11:**435–443. http://dx.doi.org/10.1016/j.ymthe.2004.10.016.
36. **Banning C, Votteler J, Hoffmann D, Koppensteiner H, Warmer M, Reimer R, Kirchhoff F, Schubert U, Hauber J, Schindler M.** 2010. A flow cytometry-based FRET assay to identify and analyse protein-protein interactions in living cells. PLoS One **5:**e9344. http://dx.doi.org/10.1371/journal.pone.0009344.
37. **Rocks O, Gerauer M, Vartak N, Koch S, Huang ZP, Pechlivanis M, Kuhlmann J, Brunsveld L, Chandra A, Ellinger B, Waldmann H, Bastiaens PI.** 2010. The palmitoylation machinery is a spatially organizing system for peripheral membrane proteins. Cell **141:**458–471. http://dx.doi.org/10.1016/j.cell.2010.04.007.
38. **Blight KJ, McKeating JA, Rice CM.** 2002. Highly permissive cell lines for subgenomic and genomic hepatitis C virus RNA replication. J Virol **76:**13001–13014. http://dx.doi.org/10.1128/JVI.76.24.13001-13014.2002.
39. **Wakita T, Pietschmann T, Kato T, Date T, Miyamoto M, Zhao Z, Murthy K, Habermann A, Krausslich HG, Mizokami M, Bartenschlager R, Liang TJ.** 2005. Production of infectious hepatitis C virus in tissue culture from a cloned viral genome. Nat Med **11:**791–796. http://dx.doi.org/10.1038/nm1268.
40. **Kato T, Date T, Murayama A, Morikawa K, Akazawa D, Wakita T.** 2006. Cell culture and infection system for hepatitis C virus. Nat Protoc **1:**2334–2339. http://dx.doi.org/10.1038/nprot.2006.395.
41. **Owsianka A, Tarr AW, Juttla VS, Lavillette D, Bartosch B, Cosset FL, Ball JK, Patel AH.** 2005. Monoclonal antibody AP33 defines a broadly neutralizing epitope on the hepatitis C virus E2 envelope glycoprotein. J Virol **79:**11095–11104. http://dx.doi.org/10.1128/JVI.79.17.11095-11104.2005.
42. **Brachet V, Pehau-Arnaudet G, Desaymard C, Raposo G, Amigorena S.** 1999. Early endosomes are required for major histocompatibility complex class II transport to peptide-loading compartments. Mol Biol Cell **10:**2891–2904. http://dx.doi.org/10.1091/mbc.10.9.2891.
43. **Pond L, Watts C.** 1997. Characterization of transport of newly assembled, T cell-stimulatory MHC class II-peptide complexes from MHC class II compartments to the cell surface. J Immunol **159:**543–553.

44. **Shaner NC, Campbell RE, Steinbach PA, Giepmans BN, Palmer AE, Tsien RY.** 2004. Improved monomeric red, orange and yellow fluorescent proteins derived from Discosoma sp. red fluorescent protein. Nat Biotechnol **22:**1567–1572. http://dx.doi.org/10.1038/nbt1037.
45. **Deleersnyder V, Pillez A, Wychowski C, Blight K, Xu J, Hahn YS, Rice CM, Dubuisson J.** 1997. Formation of native hepatitis C virus glycoprotein complexes. J Virol **71:**697–704.
46. **Vieyres G, Thomas X, Descamps V, Duverlie G, Patel AH, Dubuisson J.** 2010. Characterization of the envelope glycoproteins associated with infectious hepatitis C virus. J Virol **84:**10159–10168. http://dx.doi.org/10.1128/JVI.01180-10.
47. **Gastaminza P, Kapadia SB, Chisari FV.** 2006. Differential biophysical properties of infectious intracellular and secreted hepatitis C virus particles. J Virol **80:**11074–11081. http://dx.doi.org/10.1128/JVI.01150-06.
48. **Wölk B, Büchele B, Moradpour D, Rice CM.** 2008. A dynamic view of hepatitis C virus replication complexes. J Virol **82:**10519–10531. http://dx.doi.org/10.1128/JVI.00640-08.
49. **Shulla A, Randall G.** 2015. Spatiotemporal analysis of hepatitis C virus infection. PLoS Pathog **11:**e1004758. http://dx.doi.org/10.1371/journal.ppat.1004758.
50. **Eyre NS, Fiches GN, Aloia AL, Helbig KJ, McCartney EM, McErlean CS, Li K, Aggarwal A, Turville SG, Beard MR.** 2014. Dynamic imaging of the hepatitis C virus NS5A protein during a productive infection. J Virol **88:**3636–3652. http://dx.doi.org/10.1128/JVI.02490-13.
51. **Counihan NA, Rawlinson SM, Lindenbach BD.** 2011. Trafficking of hepatitis C virus core protein during virus particle assembly. PLoS Pathog **7:**e1002302. http://dx.doi.org/10.1371/journal.ppat.1002302.
52. **Niers JM, Kerami M, Pike L, Lewandrowski G, Tannous BA.** 2011. Multimodal in vivo imaging and blood monitoring of intrinsic and extrinsic apoptosis. Mol Ther **19:**1090–1096. http://dx.doi.org/10.1038/mt.2011.17.
53. **Chua PK, Wang RY, Lin MH, Masuda T, Suk FM, Shih C.** 2005. Reduced secretion of virions and hepatitis B virus (HBV) surface antigen of a naturally occurring HBV variant correlates with the accumulation of the small S envelope protein in the endoplasmic reticulum and Golgi apparatus. J Virol **79:**13483–13496. http://dx.doi.org/10.1128/JVI.79.21.13483-13496.2005.
54. **Stanley P.** 2011. Golgi glycosylation. Cold Spring Harb Perspect Biol **3:**a005199. http://dx.doi.org/10.1101/cshperspect.a005199.
55. **Lai CK, Jeng KS, Machida K, Lai MM.** 2010. Hepatitis C virus egress and release depend on endosomal trafficking of core protein. J Virol **84:**11590–11598. http://dx.doi.org/10.1128/JVI.00587-10.
56. **Benedicto I, Gondar V, Molina-Jimenez F, Garcia-Buey L, Lopez-Cabrera M, Gastaminza P, Majano PL.** 2015. Clathrin mediates infectious hepatitis C virus particle egress. J Virol **89:**4180–4190. http://dx.doi.org/10.1128/JVI.03620-14.
57. **Lai CK, Saxena V, Tseng CH, Jeng KS, Kohara M, Lai MM.** 2014. Nonstructural protein 5A is incorporated into hepatitis C virus low-density particle through interaction with core protein and microtubules during intracellular transport. PLoS One **9:**e99022. http://dx.doi.org/10.1371/journal.pone.0099022.
58. **Presley JF, Cole NB, Schroer TA, Hirschberg K, Zaal KJ, Lippincott-Schwartz J.** 1997. ER-to-Golgi transport visualized in living cells. Nature **389:**81–85. http://dx.doi.org/10.1038/38001.
59. **Barbero P, Bittova L, Pfeffer SR.** 2002. Visualization of Rab9-mediated vesicle transport from endosomes to the trans-Golgi in living cells. J Cell Biol **156:**511–518. http://dx.doi.org/10.1083/jcb.200109030.
60. **Liscum L, Faust JR.** 1989. The intracellular transport of low density lipoprotein-derived cholesterol is inhibited in Chinese hamster ovary cells cultured with 3-beta-[2-(diethylamino)ethoxy]androst-5-en-17-one. J Biol Chem **264:**11796–11806.
61. **Gatta AT, Wong LH, Sere YY, Calderon-Norena DM, Cockcroft S, Menon AK, Levine TP.** 2015. A new family of StART domain proteins at membrane contact sites has a role in ER-PM sterol transport. eLife **4:**e07253. http://dx.doi.org/10.7554/eLife.07253.
62. **Takano T, Tsukiyama-Kohara K, Hayashi M, Hirata Y, Satoh M, Tokunaga Y, Tateno C, Hayashi Y, Hishima T, Funata N, Sudoh M, Kohara M.** 2011. Augmentation of DHCR24 expression by hepatitis C virus infection facilitates viral replication in hepatocytes. J Hepatol **55:**512–521. http://dx.doi.org/10.1016/j.jhep.2010.12.011.
63. **Hunziker W, Whitney JA, Mellman I.** 1992. Brefeldin A and the endocytic pathway. Possible implications for membrane traffic and sorting. FEBS Lett **307:**93–96.
64. **Sáenz JB, Sun WJ, Chang JW, Li J, Bursulaya B, Gray NS, Haslam DB.** 2009. Golgicide A reveals essential roles for GBF1 in Golgi assembly and function. Nat Chem Biol **5:**157–165. http://dx.doi.org/10.1038/nchembio.144.
65. **Goueslain L, Alsaleh K, Horellou P, Roingeard P, Descamps V, Duverlie G, Ciczora Y, Wychowski C, Dubuisson J, Rouille Y.** 2010. Identification of GBF1 as a cellular factor required for hepatitis C virus RNA replication. J Virol **84:**773–787. http://dx.doi.org/10.1128/JVI.01190-09.
66. **Moradpour D, Evans MJ, Gosert R, Yuan Z, Blum HE, Goff SP, Lindenbach BD, Rice CM.** 2004. Insertion of green fluorescent protein into nonstructural protein 5A allows direct visualization of functional hepatitis C virus replication complexes. J Virol **78:**7400–7409. http://dx.doi.org/10.1128/JVI.78.14.7400-7409.2004.
67. **McLauchlan J, Lemberg MK, Hope G, Martoglio B.** 2002. Intramembrane proteolysis promotes trafficking of hepatitis C virus core protein to lipid droplets. EMBO J **21:**3980–3988. http://dx.doi.org/10.1093/emboj/cdf414.
68. **Vassilaki N, Friebe P, Meuleman P, Kallis S, Kaul A, Paranhos-Baccala G, Leroux-Roels G, Mavromara P, Bartenschlager R.** 2008. Role of the hepatitis C virus core+1 open reading frame and core cis-acting RNA elements in viral RNA translation and replication. J Virol **82:**11503–11515. http://dx.doi.org/10.1128/JVI.01640-08.
69. **Ait-Goughoulte M, Hourioux C, Patient R, Trassard S, Brand D, Roingeard P.** 2006. Core protein cleavage by signal peptide peptidase is required for hepatitis C virus-like particle assembly. J Gen Virol **87:**855–860. http://dx.doi.org/10.1099/vir.0.81664-0.
70. **Lavie M, Goffard A, Dubuisson J.** 2007. Assembly of a functional HCV glycoprotein heterodimer. Curr Issues Mol Biol **9:**71–86.
71. **Matto M, Sklan EH, David N, Melamed-Book N, Casanova JE, Glenn JS, Aroeti B.** 2011. Role for ADP ribosylation factor 1 in the regulation of hepatitis C virus replication. J Virol **85:**946–956. http://dx.doi.org/10.1128/JVI.00753-10.
72. **Corless L, Crump CM, Griffin SD, Harris M.** 2010. Vps4 and the ESCRT-III complex are required for the release of infectious hepatitis C virus particles. J Gen Virol **91:**362–372. http://dx.doi.org/10.1099/vir.0.017285-0.
73. **Ariumi Y, Kuroki M, Maki M, Ikeda M, Dansako H, Wakita T, Kato N.** 2011. The ESCRT system is required for hepatitis C virus production. PLoS One **6:**e14517. http://dx.doi.org/10.1371/journal.pone.0014517.
74. **Ploen D, Hafirassou ML, Himmelsbach K, Sauter D, Biniossek ML, Weiss TS, Baumert TF, Schuster C, Hildt E.** 2013. TIP47 plays a crucial role in the life cycle of hepatitis C virus. J Hepatol **58:**1081–1088. http://dx.doi.org/10.1016/j.jhep.2013.01.022.
75. **Ploen D, Hafirassou ML, Himmelsbach K, Schille SA, Biniossek ML, Baumert TF, Schuster C, Hildt E.** 2013. TIP47 is associated with the hepatitis C virus and its interaction with Rab9 is required for release of viral particles. Eur J Cell Biol **92:**374–382. http://dx.doi.org/10.1016/j.ejcb.2013.12.003.
76. **Menzel N, Fischl W, Hueging K, Bankwitz D, Frentzen A, Haid S, Gentzsch J, Kaderali L, Bartenschlager R, Pietschmann T.** 2012. MAP-kinase regulated cytosolic phospholipase A2 activity is essential for production of infectious hepatitis C virus particles. PLoS Pathog **8:**e1002829. http://dx.doi.org/10.1371/journal.ppat.1002829.
77. **Bartosch B, Dubuisson J, Cosset FL.** 2003. Infectious hepatitis C virus pseudo-particles containing functional E1-E2 envelope protein complexes. J Exp Med **197:**633–642. http://dx.doi.org/10.1084/jem.20021756.
78. **Grieve AG, Rabouille C.** 2011. Golgi bypass: skirting around the heart of classical secretion. Cold Spring Harb Perspect Biol **3:**a005298. http://dx.doi.org/10.1101/cshperspect.a005298.
79. **Chwetzoff S, Trugnan G.** 2006. Rotavirus assembly: an alternative model that utilizes an atypical trafficking pathway. Curr Top Microbiol Immunol **309:**245–261.